AD-A184 432   EFFECTS OF RAINFALL ON THE SEASONAL THERMOCLINE(U)   1/1
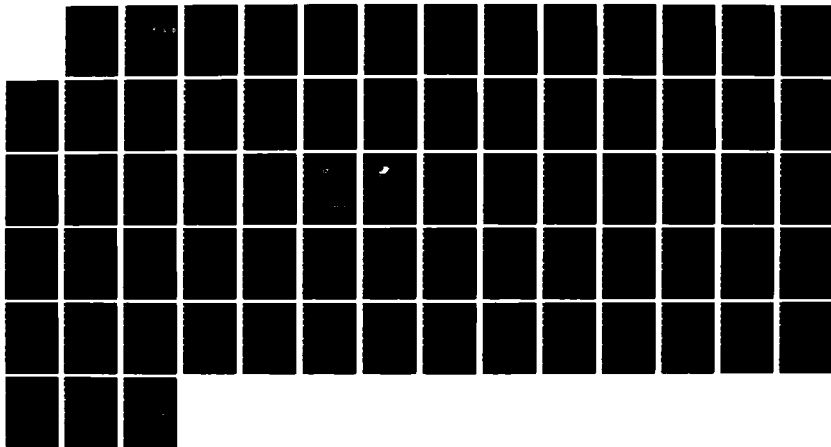NAVAL POSTGRADUATE SCHOOL MONTEREY CA   G H GARZON
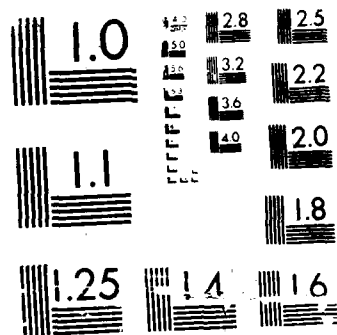JUN 87

UNCLASSIFIED   F/G 8/3   NL

1.0		2.8	2.5
		3.2	2.2
		3.6	
1.1		4.0	2.0
			1.8
1.25	1.4		1.6

MICROCOPY RESOLUTION TEST CHART

②

AD-A184 432

NAVAL POSTGRADUATE SCHOOL
Monterey, California

THESIS

EFFECTS OF RAINFALL ON THE
SEASONAL THERMOCLINE

by

Galo H. Garzon

June 1987

Thesis Advisor   R.W. Garwood

87   9   15   08

REPORT DOCUMENTATION PAGE

1a REPORT SECURITY CLASSIFICATION	1b RESTRICTIVE MARKINGS
2a SECURITY CLASSIFICATION AUTHORITY	3 DISTRIBUTION/AVAILABILITY OF REPORT
2b DECLASSIFICATION/DOWNGRADING SCHEDULE	Approved for public release; distribution is unlimited.

4 PERFORMING ORGANIZATION REPORT NUMBER(S)	5 MONITORING ORGANIZATION REPORT NUMBER(S)

6a NAME OF PERFORMING ORGANIZATION	6b OFFICE SYMBOL (If applicable)	7a NAME OF MONITORING ORGANIZATION
Naval Postgraduate School	68	Naval Postgraduate School

6c ADDRESS (City State and ZIP Code)	7b ADDRESS (City State and ZIP Code)
Monterey, California 93943-5000	Monterey, California 93943-5000

8a NAME OF FUNDING/SPONSORING ORGANIZATION	8b OFFICE SYMBOL (If applicable)	9 PROCUREMENT INSTRUMENT IDENTIFICATION NUMBER

8c ADDRESS (City State and ZIP Code)	10 SOURCE OF FUNDING NUMBERS			
	PROGRAM ELEMENT NO	PROJECT NO	TASK NO	WORK UNIT ACCESSION NO

11 TITLE (Include Security Classification)

EFFECTS OF RAINFALL ON THE SEASONAL THERMOCLINE

12 PERSONAL AUTHOR(S)
Garzon, Galo H.

13a TYPE OF REPORT	13b TIME COVERED	14 DATE OF REPORT (Year Month Day)	15 PAGE COUNT
Master's Thesis	FROM ___ TO ___	1987 June	70

16 SUPPLEMENTARY NOTATION

17	COSATI CODES		18 SUBJECT TERMS (Continue on reverse if necessary and identify by block number)
FIELD	GROUP	SUB GROUP	ocean mixed layer (model) density structure
			salinity effects salinity trend
			temperature effects

19 ABSTRACT (Continue on reverse if necessary and identify by block number)

An oceanic planetary boundary layer model is used to determine the effects of fresh water flux on the seasonal pycnocline and mixed layer at Ocean Station "P" (50°N, 145°W). First sensitivity of the model was tested by constant forcing with a range of values of precipitation minus evaporation. Then realistic forcing with daily average evaporation, monthly average precipitation values, observed winds and heat fluxes were applied to the model for a simulation of the year 1967.

The sensitivity study revealed that precipitation and evaporation have a significant impact on the seasonal evolution of mixed layer depth and temperature, even though the surface heat flux is not changed. The use of realistic forcing indicates the importance of having realistic initial salinity profiles in such models. This is especially true in

20 DISTRIBUTION/AVAILABILITY OF ABSTRACT	21 ABSTRACT SECURITY CLASSIFICATION
☒ UNCLASSIFIED/UNLIMITED ☐ SAME AS RPT ☐ DTIC USERS	Unclassified
22a NAME OF RESPONSIBLE INDIVIDUAL	22b TELEPHONE (Include Area Code)	22c OFFICE SYMBOL
Prof. R. W. Garwood	408-646-3260	68Gd

the autumn and winter seasons when rainfall reduces seasonal mixed layer deepening by as much as 25 meters, representing a 20% change. For the simulation of the year 1967, the model-predicted values of salinity very closely follow climatology for the first half of the year. During the late summer and fall, predicted salinity is greater than suggested by the climatology and may be due to unrealistically steady values of precipitation.

Effects of Rainfall on the
Seasonal Thermocline

by

Galo H. Garzon
Lieutenant J. G., Ecuadorian Navy
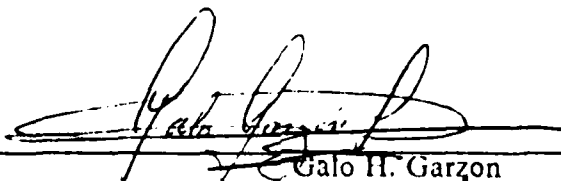Ecuadorian Naval Academy, 1981

Submitted in partial fulfillment of the
requirements for the degree of

MASTER OF SCIENCE IN METEOROLOGY AND OCEANOGRAPHY

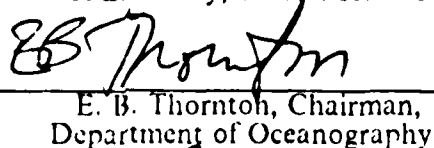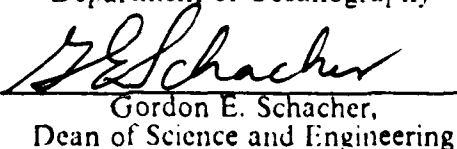
from the

NAVAL POSTGRADUATE SCHOOL
June 1987

Author: _____
Galo H. Garzon

Approved by: _____
R.W. Garwood, Thesis Advisor

_____
R.L. Haney, Second Reader

_____
E. B. Thornton, Chairman,
Department of Oceanography

_____
Gordon E. Schacher,
Dean of Science and Engineering

3

ABSTRACT

An oceanic planetary boundary layer model is used to determine the effects of fresh water flux on the seasonal pycnocline and mixed layer at Ocean Station "P" ($50°N$, $145°W$). First sensitivity of the model was tested by constant forcing with a range of values of precipitation minus evaporation. Then realistic forcing with daily average evaporation, monthly average precipitation values, observed winds and heat fluxes were applied to the model for a simulation of the year 1967.

The sensitivity study revealed that precipitation and evaporation have a significant impact on the seasonal evolution of mixed layer depth and temperature, even though the surface heat flux is not changed. The use of realistic forcing indicates the importance of having realistic initial salinity profiles in such models. This is especially true in the autumn and winter seasons when rainfall reduces seasonal mixed layer deepening by as much as 25 meters, representing a 20% change. For the simulation of the year 1967, the model-predicted values of salinity very closely follow climatology for the the first half of the year. During the late summer and fall, predicted salinity is greater than suggested by the climatology and may be due to unrealistically steady values of precipitation.

4

TABLE OF CONTENTS

5

6

LIST OF TABLES

LIST OF FIGURES

ACKNOWLEDGEMENTS

The author wishes to express gratitude and thanks to Dr. Roland W. Garwood, Jr. for his time, interest, expert guidance and encouragement during the preparation of this thesis. A very special thanks to Dr. Patrick C. Gallagher for spending his valuable time in helpful discussions.

Finally, and most certainly, I give my deepest love and gratitude to my wife, Geovanna and to my daughters, Adriana, Erika and Andrea, for their comprehension, patience and love which made the completion of this thesis possible.

I. INTRODUCTION

The upper layer of the ocean responds to atmospheric forcing on seasonal, synoptic and diurnal time scales Garwood (1977) [Ref. 1]. Krauss and Turner (1967) [Ref. 2] were the first to model the development of a thermally homogeneous oceanic mixed layer by assuming that the heat input at the air-sea interface and the mass entrainment at the bottom of the layer are mixed uniformly throughout the layer in a time scale short relative to those longer time scales of interest for prediction.

The wind stress at the ocean surface generates turbulent kinetic energy which does work against the buoyancy forces, thus increasing the potential energy in the mixed layer. The model predicts the discontinuity in temperature and density that occurs at the bottom of the mixed layer that is caused by the deepening of the mixed layer, the rate of which is inversely proportional to the magnitude of the density jump. The Krauss and Turner model [Ref. 2] was tuned by Denman (1973) [Ref. 3] and was used by Denman and Miyake (1973) [Ref. 4] to predict sea surface temperature for a 12-day period at Ocean Station "P" in the Pacific Ocean ($50°N$, $145°W$). This was the first simulation of the oceanic mixed layer at Ocean Station "P", and their predictions were well-verified by actual observations for this short period of 12 days. The effect of salinity in their short period case was insignificant because the salinity was constant to a depth of 60 meters, and the thermal mixed layer was always less than 60 meters deep.

At the air-sea interface a salinity flux occurs as a result of precipitation and evaporation. At the bottom of the mixed layer, a salinity flux is due to entrainment of water having a different salinity. Miller (1976) [Ref. 5] was the first to include salinity in a mixed layer model. Using BOMEX Period III upper ocean soundings for periods as long as 10 days, Miller showed the effects of salinity on mixed-layer temperatures and depths and the effects of precipitation on surface salinity and temperature in the tropical Atlantic. Miller studied three different cases in the deepening regime. Two of the cases concerned the heating and cooling characteristics of the mixed layer itself, while the third case dealt with the thermal relationship between the mixed layer and the region below. Miller showed that if the mixed layer salinity is greater than the salinity immediately below the mixed layer, convective overturning may occur because of a density instability unless a sufficiently large temperature decrease also occurs across the

10

interface. A large density jump significantly slows the deepening rate of the mixed layer because it leads to an appreciable increase in potential energy with only a small amount of deepening. With a net downward heat flux at the surface, the mixed layer tends to warm. However, at the bottom of the layer colder water is entrained by the deepening mixed layer and this tends reduce the lyer temperature. Without salinity flux effects, the cooling due to entrainment is often greater than the heating from the surface, and the layer may experience a net cooling. With salinity included, the layer may deepen more slowly and entrain less cold water at the bottom, causing the surface heating to dominate, and the mixed layer temperature to increase. When precipitation occurs in conjunction with high surface winds, Miller showed that the new mixed layer is deeper than at lower wind speeds. The effect of light precipitation accompanied by large surface winds cannot be detected by changes in surface salinity or temperature. However, heavy rainfall accompanied by light winds can lead to temperature and salinity decreases in significant amounts. Miller concluded that the most significant effect of inclusion of salinity was the reduced cooling rate of the mixed layer due to reduced entrainment of water from the pycnocline into the base of the layer. This type of density structure can also lead to a temperature inversion (temperature increasing with depth) immediately below the mixed layer. Miller also concluded that the short-term effects of precipitation were greatest under conditions of light winds and heavy rainfall during which a shallow stable layer is produced at the ocean surface.

Considering Miller's findings, it is apparent that salinity is only occasionally important in determining the density structure for synoptic time scales. It is hypothesized here, however that although the relative importance of salinity effects on the short term evolution of the density profile may not be significant, a long term imbalance between evaporation and precipitation may contribute to the buoyancy structure and could lead to significant changes in seasonal-scale mixed layer evolution.

R. Paulus (1978) [Ref. 6]. studied the effects of a salinity profile on density structure and the added effects of surface salinity flux for a period of two months. Paulus showed that the inclusion of salinity structure in a one dimensional model of ocean thermal structure did not significantly affect mixed layer depth or temperature prediction during the summer period. During the winter period, Paulus showed that salinity structure tended to inhibit deepening, yielding a slightly warmer, and shallower mixed layer. He concluded that surface salinity flux could significantly alter the thickness of the isothermal layer during precipitation, and he predicted a tendency for

11

increased thickness during some periods of net downward heat flux when evaporation exceeds precipitation.

II. THEORY

A. SURFACE OCEANIC PLANETARY BOUNDARY LAYER

The ocean mixed layer is assumed here to be coincident with the fully turbulent region of the upper ocean that is bounded above by the sea-air interface, and below by a dynamically stable watermass. The wind and buoyancy flux through the surface are the sources of mechanically energy for the generation of this turbulence.

According to Krauss and Turner (1967) [Ref. 2] the mixed layer is considered to be quasi-homogeneous (mathematically approximated to be well mixed). Below this turbulent boundary layer, the water column is hydrostatically stable. See Figure 2.1 Region I is the fully turbulent mixed layer of depth h. and region II is the slightly stable, intermittently turbulent entrainment zone of thickness δ Region III is the stable underlying watermass having vertical fluxes negligible in comparison to those of region I.

The prediction or the rate of deepening (or retreat) at the mixed layer is dependent upon an understanding of the dynamics of the entrainment process. It is assumed that the turbulence of the overlying mixed layer provides the energy needed to destabilize and erode the underlying stable water mass in accordance with Garwood (1977) [Ref. 1].

Due to mechanical mixing at the surface, temperature, salinity, density and consequently mixed layer depth as well as the thickness of the entrainment or transition zone will all change in time. From Figure 2.1, the conservation of heat requires that:

$$(\Delta T)(\delta h) = (h)(-\delta T) \tag{2.1}$$

or

$$\delta T = -(\Delta T)(\delta h)/h. \tag{2.2}$$

The discontinuity $\Delta \overline{T} = \overline{T} - \overline{T}(z=-h)$, where T is the mixed layer temperature. $T(z=-h)$ is the temperature immediately below the mixed layer, and δT is the

13

Figure 2.1   Idealized temperature and mean velocity profiles..

temperature reduction due to entrainment. In the entrainment process, Equation (2.2) becomes:

$$\frac{\partial T}{\partial t} = -\frac{\Delta T}{h}\frac{\partial h}{\partial t} , \tag{2.3}$$

which can be recognized as the First Law of Thermodynamics. The time derivative, $\partial h \, \partial t = W_e$, is the entrainment velocity. In general $\partial h/\partial t$ depends also on the vertical velocity or advection,

$$\frac{\partial h}{\partial t} = W_e - W(-h) \tag{2.4}$$

14

The entrainment heat flux is $-\Delta T\, W_e = \overline{T'W'}(-h)$. The entrainment heat flux must be less than or equal to zero if $\Delta T > 0$.

Considering now the vertical exchange of heat for a turbulent fluid:

$$\int_{-h.-\delta}^{0} \frac{\partial \overline{T}}{\partial t}\, dz = \int_{-h.-\delta}^{0} \frac{-\partial(\overline{T'W'})}{\partial z}\, dz \tag{2.5}$$

Solving the integrals:

$$\frac{\partial T}{\partial t} = \frac{\overline{T'W'}(0)}{h} + \frac{\overline{T'W'}(-h)}{h} \text{ , or} \tag{2.6}$$

$$\frac{\partial T}{\partial t} = \frac{\Delta T.W}{h}_e + \frac{Q_0 (\rho C_p)}{h}. \tag{2.7}$$

Where $\Delta \overline{T} = \overline{T} - \overline{T}(-h-\delta)$, and $Q_0/\rho C_p = -\overline{T'W'}(0)$. To close the problem, an equation for W_e needs to be derived to predict $h(t)$.

A useful simple model for W_e is that of Kraus and Turner (1967) [Ref. 2] who suggested:

$$W_e = [C_1\, U_*^3 - C_2\, \alpha\, g\, h\, (Q_0/\rho\, C_p)h]/(\alpha\, g\, h\, \Delta T) \tag{2.8}$$

Although this equation will be replaced by an improved turbulence closure model [Garwood, (1977)] [Ref. 1] in the actual investigations undertaken in this research. Equation (2.8) is useful for scale analysis and to demonstrate how the inclusion of salinity changes the functional form of the entrainment equation.

1. Entrainment "Jump Condition" For Salinity

The mixed layer depth h is the distance over which turbulent energy must be transported by the vertical component of turbulent velocity. The one-dimensional salinity budget is:

15

$$\partial S / \partial t = -\partial (W'S') / \partial z. \tag{2.9}$$

Three assumptions are made:

(i) S(z) is well mixed between the surface and the bottom of the mixed layer (z = 0, and z = -h).

(ii) S(z) has a near discontinuity between z = -h, and z = -h-δ, δ < < h.

(iii) The vertical flux of S, S'W', vanishes at z $\leq$ -h-δ.

Figure 2.2 shows the assumed S(z).

Figure 2.2   Assumed S(z) Distribution in Mixed Layer.

This assumption is based on the reduced level or absence of turbulence below the mixed layer. The distribution of S does not have to be perfectly homogeneous above z = -h, but it does have to be much more well-mixed than it is below the mixed layer. Vertically integrating, Equation (2.9) across the entrainment zone gives Equation (2.10). Since h is variable in time, Leibnitz Rule of integration applies here [see

16

Equation (2.11)]. For our problem, a = -h(t), and b = -h(t)-δ Therefore, Equation (2.12).

$$\int_{-h(t)-\delta}^{-h(t)} \frac{\partial \overline{S}}{\partial t} dz = \int_{h-\delta}^{-h} \frac{\partial \overline{W'S'}}{\partial z} dz \tag{2.10}$$

$$\int_{b(t)}^{a(t)} \frac{\partial F}{\partial t} = \frac{\partial}{\partial t} \int_{b}^{a} F \, dz - F(z=a)\frac{\partial a}{\partial t} + F(z=b)\frac{\partial b}{\partial t} \tag{2.11}$$

$$\frac{\partial}{\partial t} \int_{-h-\delta}^{-h} S \, dz + S(z=-h)\frac{\partial h}{\partial t} - S(-h-\delta)\frac{\partial h}{\partial t} \quad , \tag{2.12}$$

provided that δ does not change in time ($\delta \neq \delta(t)$, or is small compared to h, then $S(-h) \, \partial h \, \partial t - S(-h-\delta) \, \partial h/\partial t = \Delta S \, \partial h/\partial t$.

The first term of Equation (2.12) is $\partial/\partial t - (S-\Delta S/2) = <S>$. For a perfect discontinuity $\delta \sim 0$, $<S>$ is the approximate average of S over the small entrainment zone, and $\Delta \overline{S} \, \partial h \, \partial t = -\overline{W'S'}(-h) + \overline{W'S'}(-h-\delta) + a(S \, \delta)$. If turbulence is negligible below the mixed layer, $\overline{W'S'}(-h-\delta) \sim 0$. Therefore, the "jump condition" for entrainment of salinity into the mixed layer reduces to:

$$\Delta \overline{S} \, \partial h \, \partial t = -\overline{W'S'}(-h). \tag{2.13}$$

2. Effect of Salinity on the Equilibrium Solution

Assume a steady state balance between the work done by the wind stress and the buoyant damping, so that $W_e = 0$. Furthermore assume no vertical advection, $W(-h) = 0$. Then the entrainment model, Equation (2.8) reduces to:

$$W_e = C_1 \, U^3 \, (\alpha \, g \, h \, \Delta T) - C_2 \, Q_0 \, (\rho \, C_p \, \Delta T) = 0 \quad , \tag{2.14}$$

which is a diagnostic equation for mixed layer depth,

17

$$h = \frac{C_+}{C_2^+} \frac{U^{-3}}{[\alpha g Q_0 (\rho C_p)]} = L \qquad (2.15)$$

Here L is the Obukhov length scale. Equation (2.15) is the solution when there is no entrainment, where $[\alpha g q_0'(\rho C_p)] = B_0$ is the surface buoyancy flux. Because h is inversely proportional to Q_0, the mixed layer temperature is even more strongly affected by Q_0 than is h:

$$\partial T / \partial t = Q_0'(\rho C_p h) \propto Q^2. \qquad (2.16)$$

Including a surface salinity flux, $S'W'(0) = S(E-P)$, and assuming a steady state balance between the work done by the wind stress and the buoyant damping and no vertical advection, the mixed layer depth equation reduces to:

$$h = \frac{C_+}{C_2^+} \frac{U^{-3}}{[\alpha g Q_0'(\rho C_p) + \beta g (P-E) S]} , \qquad (2.17)$$

where $\beta = 0.76 * 10^{-3}$ kg/gm and E-P is net evaporation minus precipitation in m/sec. Equation (2.17) is the solution when there is no entrainment. With salinity included the total surface buoyancy flux is:

$$B_0 = [\alpha g Q_0'(\rho C_p) + \beta g (P-E) S]. \qquad (2.18)$$

The predicted effect on mixed layer temperature is:

$$\partial T / \partial t = (Q_0'\rho C_p)/h \propto Q_0[Q_0 + \beta \alpha (P-E) S]. \qquad (2.19)$$

From Equation (2.19), even considering the incoming solar radiation as a constant, it is apparent that precipitation minus evaporation (P-E) influences temperature indirectly by affecting mixed layer depth. If precipitation exceeds evaporation, a positive value of (P-E) is generated which increases the temperature with time. The opposite is true when evaporation is greater than precipitation. Using the linearized Equation of State, $\alpha g \Delta T$ can be replaced by ΔB:

18

$$\Delta B = \alpha \, g \, \Delta T - \beta \, g \, \Delta S \quad , \tag{2.20}$$

$\Delta \overline{S} = \overline{S} - \overline{S}(- h - \delta)$, where β is the thermal expansion coefficient, ΔS is the salinity discontinuity $\Delta \overline{S} = \overline{S} - \overline{S}(-h - \delta)$. S is the mixed layer salinity. $S(-h - \delta)$ is the salinity immediately below the mixed layer. The mixed layer salinity budget is:

$$\frac{\partial S}{\partial t} = \frac{S(E - P) - W_e \, \Delta S}{h} \quad . \tag{2.21}$$

Equation (2.21) shows that the change in salinity with time directly depends on both the fresh water flux and the entrainment velocity.

3. Entrainment and Turbulent Kinetic Energy Equation

Although the Kraus-Turner model Equation (2.8), was useful for a simplified analysis of the effect of salinity on the turbulent entrainment problem, a more realistic turbulence closure method will be used for quantifying the importance of salinity in the real ocean. The turbulent kinetic energy (TKE) budget is the basis for the improved model. The TKE equation is:

$$\frac{\partial \overline{E}}{\partial t \, 2} = \{-\overline{U'W'}\frac{\partial U}{\partial z} - \overline{V'W'}\frac{\partial V}{\partial z}\} + [\alpha g \overline{T'W'}] - \frac{\partial}{\partial}\{\overline{W'(\frac{E}{2} + \frac{P'}{\rho_0})}\} - \varepsilon \tag{2.22}$$

where $E = U'^2 + V'^2 + W'^2$.

The time rate of change of turbulent kinetic energy is usually the smallest term and can be neglected. The shear production term, $[-\overline{u'w'}\partial U \, \partial z - \overline{v'w'}\partial V \, \partial z]$, which represents the rate of mechanical production is often the dominant source of TKE. The vertical temperature flux, $T'W'$, is either a source or sink for TKE, depending upon its sign. In the case of a downward heat flux during the day, $\overline{T'W'} < 0$ destroys turbulence. However, at night $T'W'$ is usually negative, creating turbulence by free convection. The divergence of the turbulent flux of KE or turbulent diffusion is. $-\partial \, \partial z [\overline{W'(E/2 + P' \rho_0)}]$. Locally, at the bottom of the layer during occasions of entrainment, a net convergence of flux of energy is necessary to maintain the downward buoyancy flux for deepening the mixed layer. The term ε represents viscous dissipation. Because of the local isotropy, ε is assumed divided equally among the

19

component TKE budgets. In the entrainment zone at the base of the mixed layer, Equation (2.22) reduces to Equation (2.23).

$$\frac{\partial}{\partial t} \left. \frac{E}{2} \right\rfloor_{h} = \; \sim \; \alpha \, g \, \overline{T'W'} \rfloor_{h} \, \frac{\partial}{\partial z} \overline{[W'(\frac{E}{2} + \frac{P'}{\rho_0})]} \rfloor_{h} \tag{2.23}$$

For finite ΔT, the growth of the internal boundary layer is slow, so $\partial \partial t (E\,2)_{-h}$ may be negligible. Since the convergence of flux of turbulent energy at the interface is primarily responsible for the entrainment buoyancy flux, it is necessary to estimate the time scale τ_v required to transport a portion of the available turbulent energy (E) to the vicinity of the entrainment interface:

$$-\frac{\partial}{\partial z} \overline{[W'(\frac{E}{2} + \frac{P'}{\rho_0})]} \rfloor_{h} = \; \frac{\overline{E}}{\tau_v} \quad , \tag{2.24}$$

Where $E \tau_v = \sqrt{\overline{W'^2}} \, E \, h$. W' is the transport of turbulence. For large W', τ_v has to be small, and

$$\tau_v = h \sqrt{\overline{W'^2}} \tag{2.25}$$

4. TKE in the Entrainment Zone

Using Equations (2.24), (2.25) and the jump condition Equation (2.13), Equation (2.23) becomes:

$$\frac{\partial}{\partial t}(\frac{E}{2}) \rfloor_{h} = \frac{\sqrt{\overline{W'^2}} <\overline{E}>}{h} - \alpha \, g \, \Delta T \, W_e \quad , \tag{2.26}$$

where the first term of Equation (2.26) represents unsteadiness, the second term is transport, and the last term represents the entrainment buoyancy flux term which destroys turbulence.

If the unsteadiness is negligible in Equation (2.26), an expression for W_e can be derived:

Recalling that the Krauss and Turner equation for the entrainment velocity is given by:

20

$$W_e = \frac{\sqrt{\overline{W'^2}} < \overline{E} >}{h \, \alpha \, g \, \Delta T [1 + < \overline{E} > (h \, \alpha \, g \, \Delta T)]} \tag{2.27}$$

$$W_e = [C_1 \, U^3 - C_2 \, \alpha \, g \, h(Q_0 \, \rho C_p)] \cdot (h \, \alpha \, g \, \Delta T) \quad . \tag{2.28}$$

a comparison with Equation (2.27) is possible.

5. Bulk Turbulence Closure Mixed-Layer Model Equations Without Salinity

Entrainment rate

$$W_e = \frac{\sqrt{\overline{W'^2}} < \overline{E} >}{h \, \alpha \, g \, \Delta T + < \overline{E} >} \tag{2.29}$$

Mixed Layer Depth:

$$\partial h / \partial t = W_e - \overline{W}(- h) \tag{2.30}$$

Total Turbulent Kinetic Energy:

$$\frac{\partial}{\partial t}(h < \overline{E} >) = G_0 + G_h - B_0 - B_h - D \tag{2.31}$$

Vertical Turbulent Kinetic Energy:

$$\frac{\partial}{\partial t}(h < \overline{w'^2} >) = - B_0 - B_h + R - \frac{1}{3} D \tag{2.32}$$

Mixed Layer Temperature:

$$\frac{\partial}{\partial t} < \overline{T} > = \frac{Q_0 \, (\rho \, C_p) - \Delta W_e}{h} \tag{2.33}$$

21

Mixed Layer Currents [Equations (2.34) and (2.35)]:

$$\frac{\partial}{\partial t}(h <\overline{u}>) = f h < v > + \frac{\tau_x}{\rho} \tag{2.34}$$

$$\frac{\partial}{\partial t}(h <\overline{v}>) = f h < u > + \frac{\tau_y}{\rho} \tag{2.35}$$

The Shear Production at the surface, at the bottom and the Buoyant Damping Production at the surface are respectively Equations (2.36), (2.37) and (2.38):

$$G_0 = 12 \, u^3 = 12 \, [(\frac{\tau_x}{\rho})^2 + (\frac{\tau_y}{\rho})^2]^{3/4} \tag{2.36}$$

$$G_h = [<\overline{u}>^2 + <\overline{v}>^2] \, W_e \tag{2.37}$$

$$B_0 = \alpha \, g \, h \, \overline{T'W'}(0) = -\alpha \, g \, h \, Q_0 / (\rho \, C_p) \tag{2.38}$$

Buoyant Damping Production at the bottom of the layer:

$$B_h = \alpha \, g \, h \, \Delta\overline{T} \, W_e \tag{2.39}$$

Dissipation:

$$D = 2 < \overline{E} >^{3/2} \tag{2.40}$$

Redistribution:

The Temperature Jump:

or

where Γ is the lapse rate below the mixed layer.

22

$$R = 2 \left(<\overline{E}> - 3 < \overline{w'^2}> \right) \sqrt{E} \qquad (2.41)$$

$$\Delta\overline{T} = <\overline{T}> - \overline{T}(-h) \qquad (2.42)$$

$$\Delta\overline{T} = <\overline{T}> - (T_0 - \Gamma h). \qquad (2.43)$$

6. Adding Salinity to the Model

(1) $\alpha g Q_0 / (\rho C_p)$ has to be replaced with a net downward surface buoyancy flux, B_0,

$$B_0 = \alpha g [Q_0 / (\rho C_p)] - \beta g \overline{S} (E - P) \qquad (2.44)$$

where:

$\beta = 0.76 * 10^{-3}$ kg/gm,

S = mixed layer salinity (gm/kg), and

$E - P$ = evaporation - precipitation (mm/hour).

(2) Replacing $\alpha g \Delta T$ with ΔB:

$$\Delta\overline{B} = \alpha g \Delta\overline{T} - \beta g \Delta\overline{S}, \qquad (2.45)$$

where the salinity discontinuity $\Delta\overline{S} = \overline{S} - \overline{S}(-h-\delta)$

(3) Adding a salinity equation for the mixed layer:

$$\frac{\partial\overline{S}}{\partial t} = \frac{\overline{S}(E-P) - W_e \Delta\overline{S}}{h} \qquad (2.46)$$

7. Summary of Equations with Salinity

$S(z < -h)$ needs to be specified

$T(z < -h)$ needs to be specified

$$\frac{\partial h}{\partial t} = W_e - \overline{W}(- h)$$

(2.47)

$$W_e = \frac{C_1 U^3 - C_2 B_0 h}{h \Delta B^2}$$

(2.48)

$$\frac{\partial T}{\partial t} = \frac{[Q_0 / (\rho C_p)]}{h} - W_e \Delta T$$

(2.49)

$$\frac{\partial S}{\partial t} = \frac{S(E - P)}{h} - W_e \Delta S$$

(2.50)

$$\Delta \overline{S} = \overline{S} - \overline{S}(- h - \delta)$$

(2.51)

$$\Delta \overline{T} = \overline{T} - \overline{T}(- h - \delta)$$

(2.52)

$$\Delta B = \alpha g \Delta \overline{T} - \beta g \Delta \overline{S}$$

(2.53)

$$B_0 = \alpha g \frac{Q_0}{\rho C_p} - \beta g \overline{S}(E - P)$$

(2.54)

8. Model Constants

ρ_a Density of air

ρ_0 Density of sea water

α, β Thermal expansion coefficients

g Acceleration of gravity

C_p Specific heat at constant pressure

C_d Drag coefficient

24

f   Coriolis parameter (latitude dependent)

The following boundary conditions have to be prescribed hourly:

τ Wind stress   (dynes/cm^2)

Q_0 Incoming solar radiation (W/m^2)

Q_b Back radiation (W/m^2)

Q_e Latent heat flux

Q_h Sensible heat flux

E   Evaporation (mm/hour)

P   Precipitation (mm/hour)

III. HYPOTHETICAL EXPERIMENT

A. ADJUSTMENT OF THE OPBL TO AN ANNUAL HEATING CYCLE WITHOUT SALINITY FORCING

The bulk second order closure method of Garwood (1977, JPO) [Ref. 1] is employed to simulate the oceanic planetary boundary layer for a full year. The specified (hourly) boundary conditions are wind stress (τ), solar radiation (Q_s), net upward turbulent heat flux and back radiation (Q_b), evaporation (E), and precipitation (P). The predicted variables are mixed layer depth (h), temperature (T), and salinity (S). Also, the temperature profiles and salinity profiles below the mixed layer need to be specified as initial conditions

This simple hypothetical case is computed to show the relative importance of excess precipitation or of excess evaporation over a time period of at least one year. The primary question is the sensitivity of the annual cycle to a variety of prescribed values of precipitation minus evaporation (P-E), held constant for one year during which the mixed layer is experiencing an annual period heating and cooling cycle. In order to determine the sensitivity to P-E, it first is necessary to simulate the annual cycle in mixed layer depth and temperature due to surface heating alone with P-E = 0. Figure 3.1 shows the annual cycle in mixed layer depth for this case, and Figure 3.2 shows the temperature annual cycle. These results are typical for the mid-latitude mixed layer, in comparison with the climatological data from the atlas of Robinson [Ref. 7]. In order to verify that a cyclical steady state was achieved approximately, the computation was continued for a second year. Figures 3.3 and 3.4 show the second-year predictions for h and T, respectively. A comparison of the results for the two different years shows that cyclical steady state is approximated. For both years the forcing conditions and initial conditions were:

τ_0 = 0.75 dynes cm/cm (wind stress)

PME = 0. mm/hour (precipitation - evaporation)

Q_0 = 150. watts/m/m (net heat flux)

T(0) = 6°C (initial temperature)

S(0) = 34. ppm (initial salinity)

h(0) = 6000 cm (initial mixed layer depth)

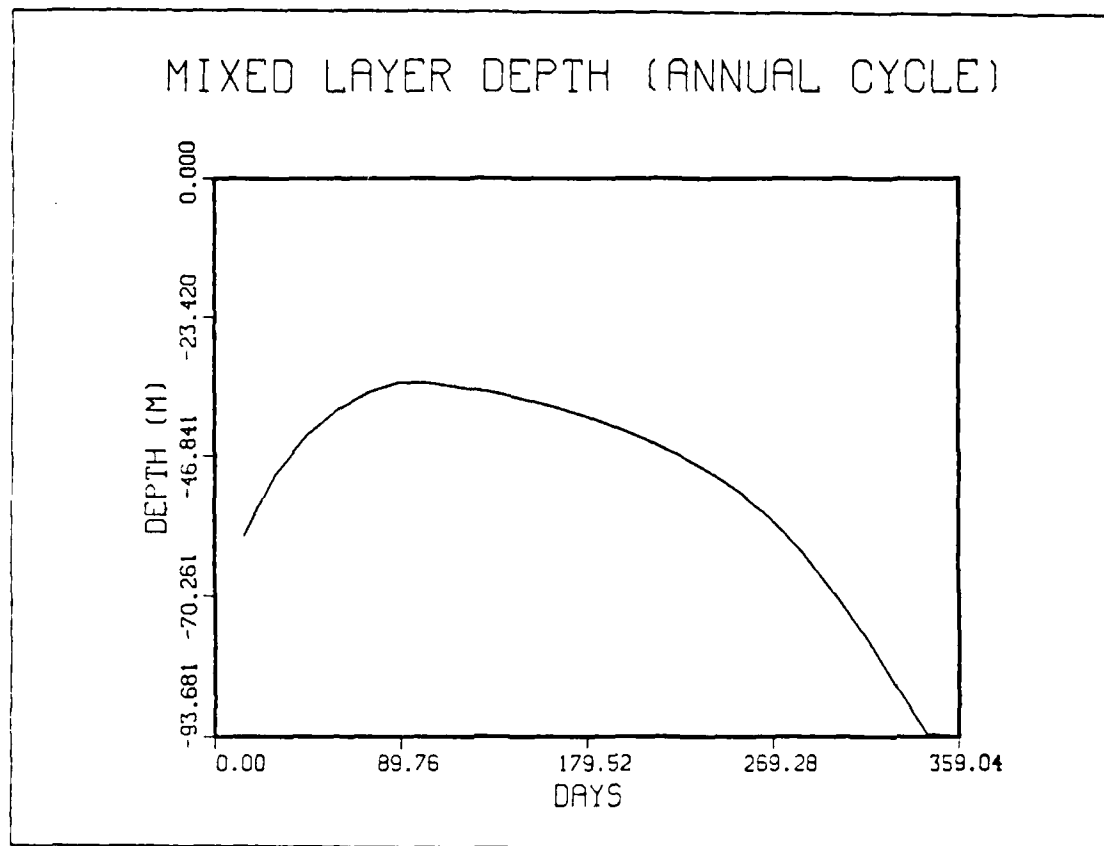AM = 2. (model constant)

AZR = P_1 = P_2 = 1. (model constants)

26

Figure 3.1   Mixed layer depth (annual cycle).

$AG = \alpha\, g = 0.2\ C^{-1}\ cm\ sec^{-2}$

With the above conditions, and with no precipitation or evaporation a slightly deeper mixed layer was observed at the end of the first year, having a value of 8971 cm. The temperature did not show a significant change, being equal to $5.48°C$ at the end of the year.

These new values of temperature ($5.48°C$), and mixed layer depth (8971 cm) were entered as initial conditions for the second year of identical surface forcing.

Figures 3.3 and 3.4 show that the mixed layer depth, starting at 89.71 meters, shallows at the beginning of the year (which for this hypothetical case is considered to be March 21, the vernal equinox) until day 90, when it then deepens slowly until day 270, the autumnal equinox. After this, during the hypothetical fall season, the mixed layer deepens faster through day 360. At the very end of the year there is shallowing again to a value of 93 meters (just before "spring"), a somewhat deeper value compared
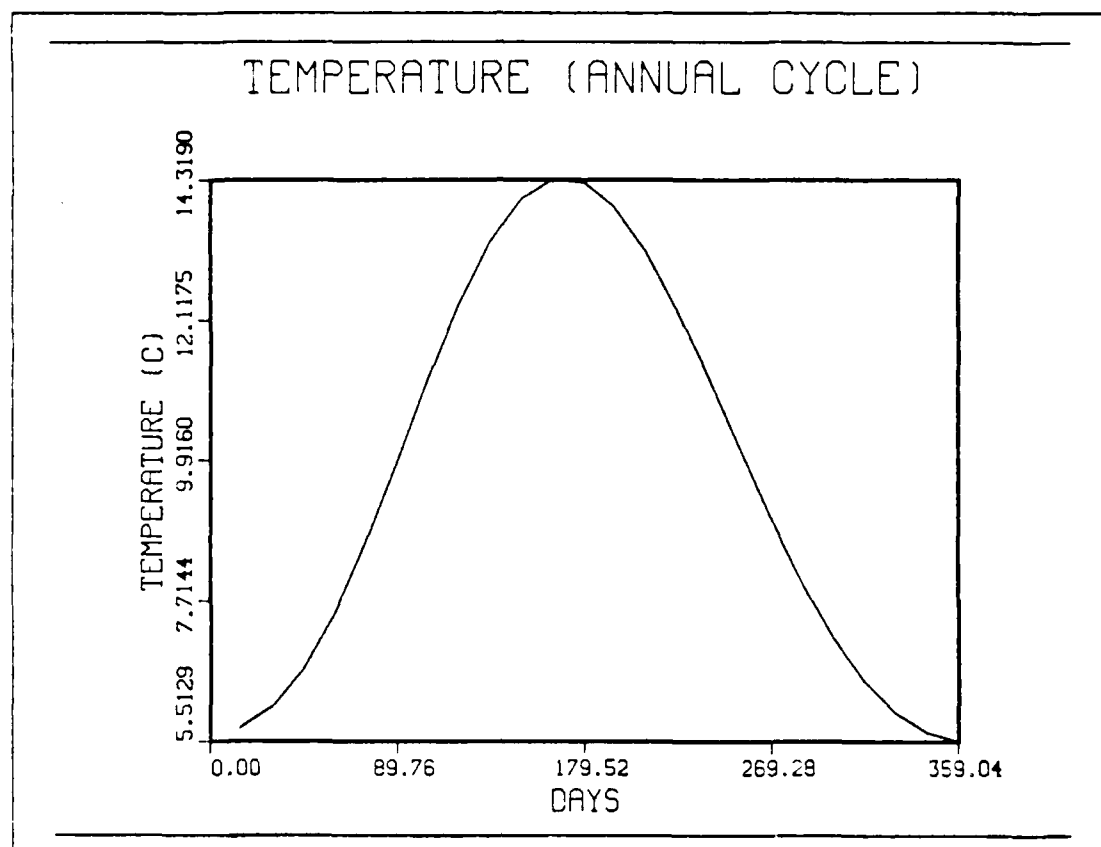
27

Figure 3.2   Temperature (annual cycle).

with the initial value of the second year. This indicates a nearly closed annual cycle is
occurring in the mixed layer depth which is in agreement with a "perfect" climatology.
Figure 3.4 shows an almost perfect annual cycle in temperature. Starting at a value of
5.48°C, the temperature gets warmer, peaking at a value of 13.71°C at day 180.
Afterwards, the temperature decreases until the end of the year, showing a slightly
colder final temperature of 4.98°C. This is in approximate agreement with the first year
computation and with climatology typical for the temperate oceans.

B.   SENSITIVITY OF THE ANNUAL CYCLE TO SALINITY FORCING

Having established the cyclical response to thermal forcing alone, net
precipitation and evaporation was added to determine the sensitivity of the OPBL to
surface fluxes of salinity. The hypothesis to be tested is that net precipitation minus
evaporation may have a significant effect on the mixed layer on seasonal and longer
time scales.

28

Figure 3.3   Second year mixed layer depth.

The mean annual rainfall at 50°N and 145°W is about 1 meter year (Dorman and Bourke, 1979) [Ref. 8]. Thus the upper bound of P-E was taken as 1 m/year. The model was forced for a full year with this rate of net precipitation. Next the model was again integrated for 20 different cases, reducing P-E by 0.1 m year for each case, but starting with identical initial conditions.

1. Results

Figure 3.5 depicts the mixed layer depth versus time for the collection of cases, with P-E varying between + 1 m year and -1 m/year. To show the sensitivity to P-E, the results in Figure 3.5 are subtracted from the P-E = 0 case, Figure 3.6.

From Figures 3.5 and 3.6, it is apparent that the initial depth for the different cases of P-E was the same 89.71 meters. For all values of P-E it begins to shallow until day 90 and then deepens rapidly, especially when P-E is negative. For the case of no precipitation and no evaporation the depth of the mixed layer starts at 89.71 m, begins

29

TEMPERATURE (ANNUAL CYCLE)

Figure 3.4   Second year temperature.

to shallow until day 90 to a value of around 35 m, then it deepens rapidly until day 345, after which it shallows to 93 meters. This is several meters deeper than the initial value.

For the cases where the evaporation is greater than precipitation, creating a net evaporation situation, the mixed layer depth anomaly increases throughout the year. As evaporation increases, the salinity first increases then drops. Thus at the begining of the year until day 90, a slight shallowing of mixed layer depth (MLD) is observed, but it is not as shallow as is the case with P-E > 0. This is due to the reduction in the downward surface buoyancy flux, causing a deeper h, as predicted by Equation (2.15). By continuously evaporating fresh water from the sea surface and by cooling, the surface water becomes denser than the water lying immediately below. As a result, the surface water sinks until it encounters water of the same density. A decrease in surface temperature and a consequent increase in salinity is observed in

30

MIXED LAYER DEPTH (CM)

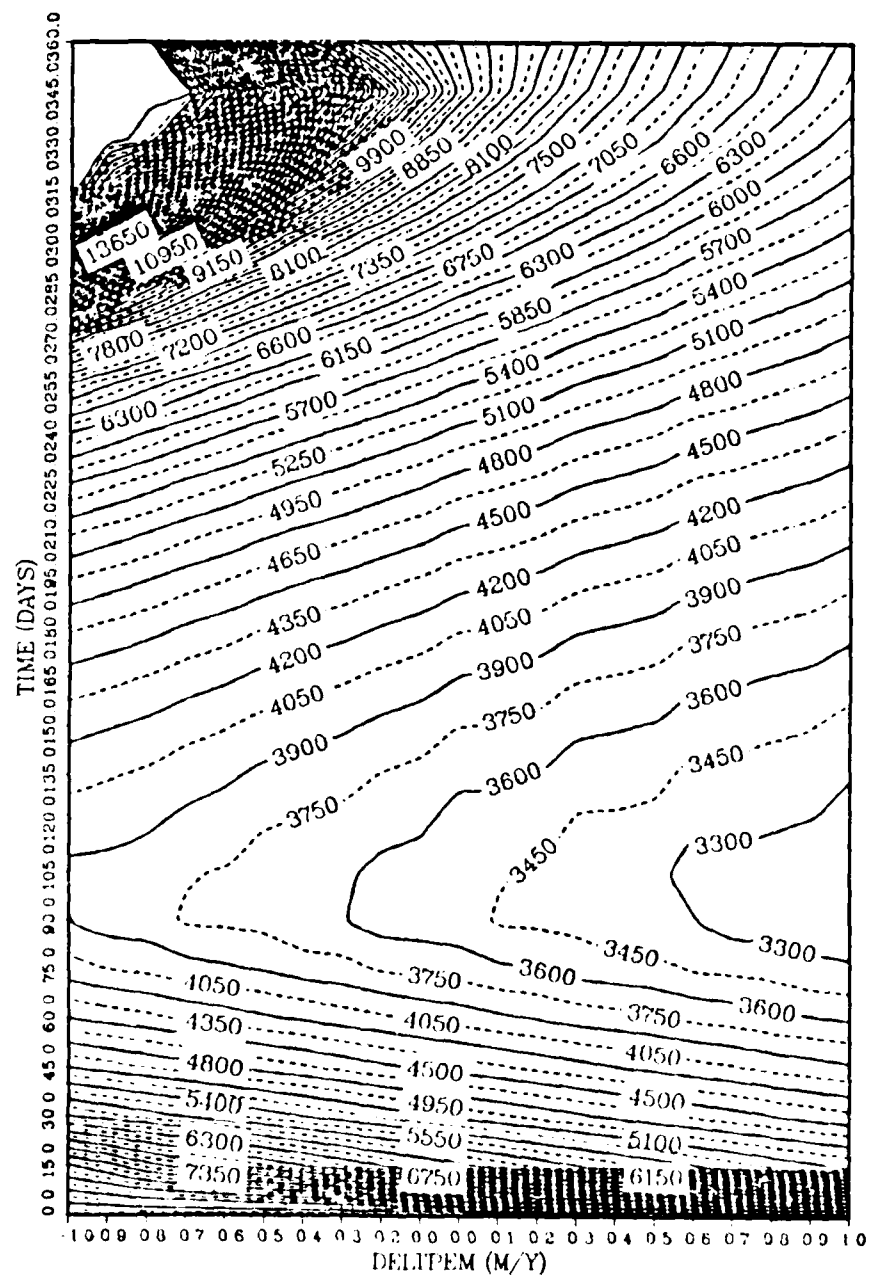
Figure 3.5 Mean annual mixed layer depth (cm).

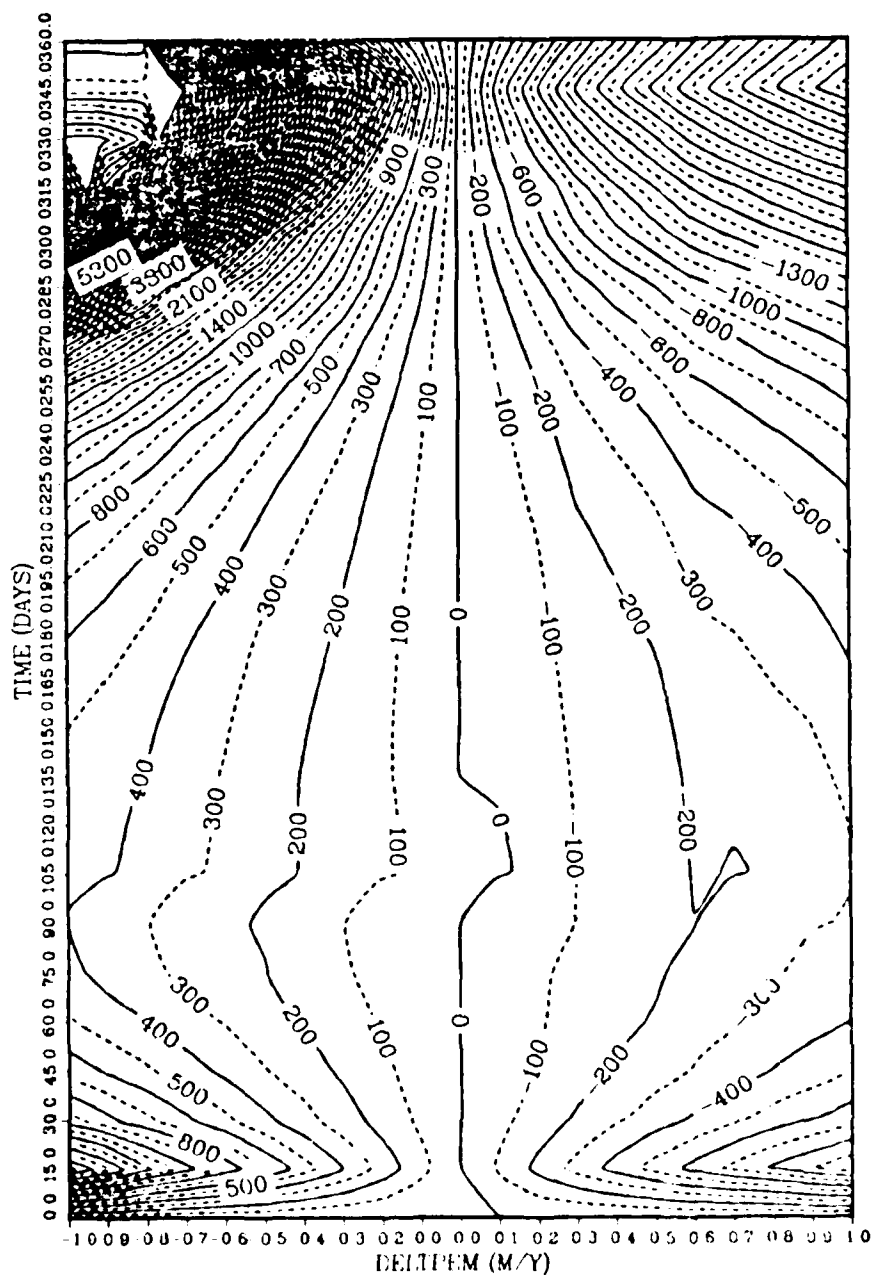31

MIXED LAYER DEPTH ANOMALY (CM)

Figure 3.6 Mean annual mixed layer depth anomaly (cm).

32

Figure 3.7, showing a more stable ocean which affects the deepening rate of the mixed layer. As an example, contrasting the values for mixed layer depth at day 90 for the cases of P-E = 0.5 m/year and P-E = -0.5 m/year, it is observed that the MLD is 37 m and 33.5 m, respectively. When there is more rain the ocean is more stratified (see Figure 3.7), and the ocean concentrates heat into a shallower depth. After day 90, when evaporation exceeds precipitation, the MLD begins to deepen very rapidly and this brings water with lower salinity to the surface, diluting the surface salinity. The net result is a very rapid deepening rate of the mixed layer until day 345. This completes the annual cycle.

When P-E = -0.7 m/year or less the MLD reaches the bottom of the model ocean, and the results are not relevant to the real ocean after day 315. For the case of P-E = -0.5 m/year, the MLD at the end of the year is greater than 100 meters. This is because the salinity at the surface increases continuousiy due to constant evaporation. This higher salinity water will entrain further into the thermocline, creating a mixed layer deeper than the initial value. When there is more rain than evaporation, the mixed layer after day 90 deepens more slowly than when evaporation is taken into account because turbulence is dampened as predicted by Equations (2.44) and (2.48). However, the dilution effect is not as large as it is in the evaporation case because increased stability also reduces entrainment. For the case of P-E = 0.5 m/year, after day 90 the mixed layer deepens until day 345. It continues deepening but at a slightly slower rate than before, reaching a depth of 73.5 meters at the end of the model year. This value is shallower than the initial value of 89.71 meters, as was expected.

Figure 3.6 depicts the mixed layer depth anomaly (relative to the P-E = 0 case) throughout the year. When evaporation exceeds precipitation, the anomaly increases until day 15 after which it begins to decrease until day 90, resulting in a net shallowing of the mixed layer. The MLD then increases until day 345, after which it decreases again. For 0.5 m/year of net evaporation, the anomaly value at the end of the cycle is greater than 20 meters, indicating that the MLD is greater than the initial value. When there is a net precipitation, the anomaly (negative in this case showing a MLD less deeper than the initial value) decreases until day 15. It then increases until day 90, after which it decreases until day 345. Subsequently the anomaly starts to increase again. For 0.5 m/year of net precipitation, the anomaly at the end of the cycle is -19 meters indicating that the MLD is shallower than the initial value.
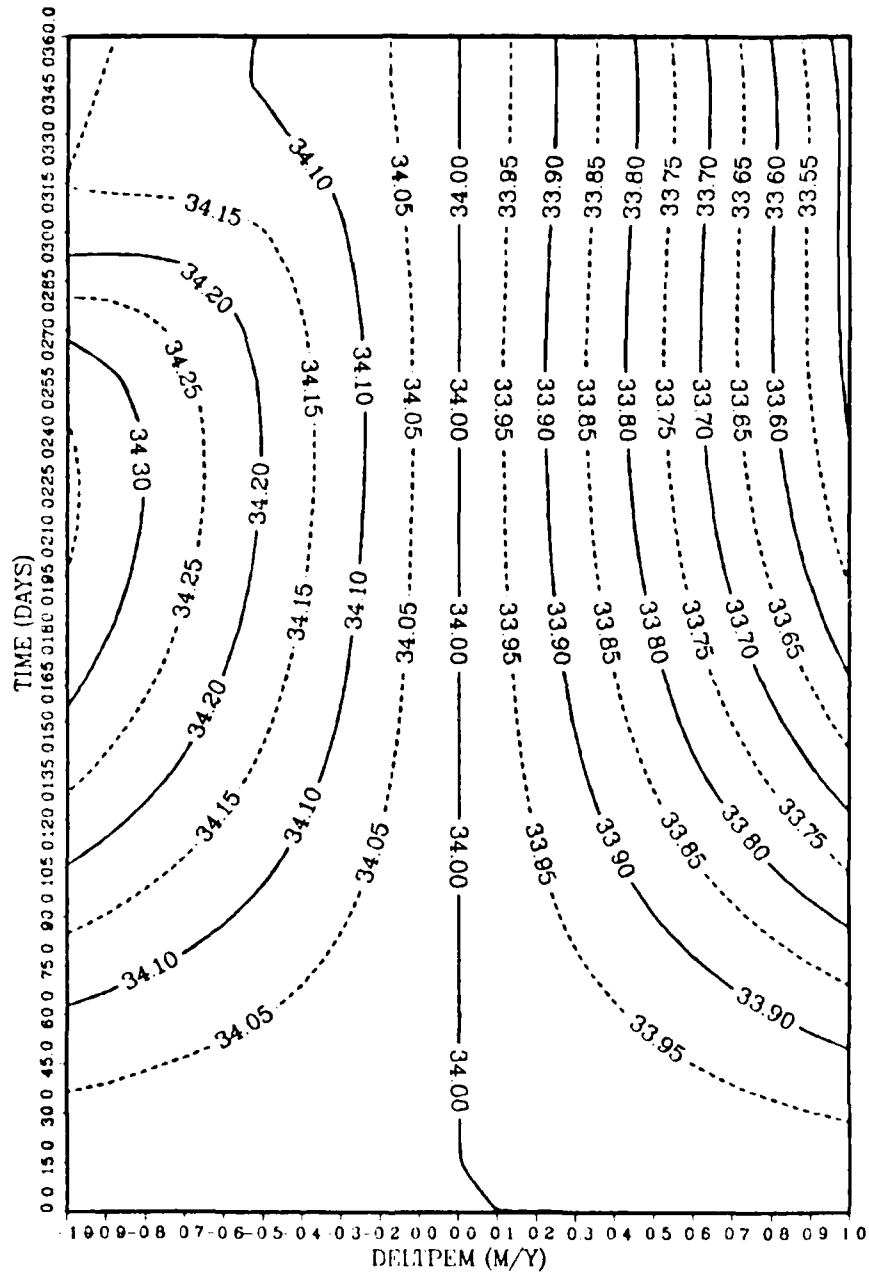
33

SALINITY (PPM)

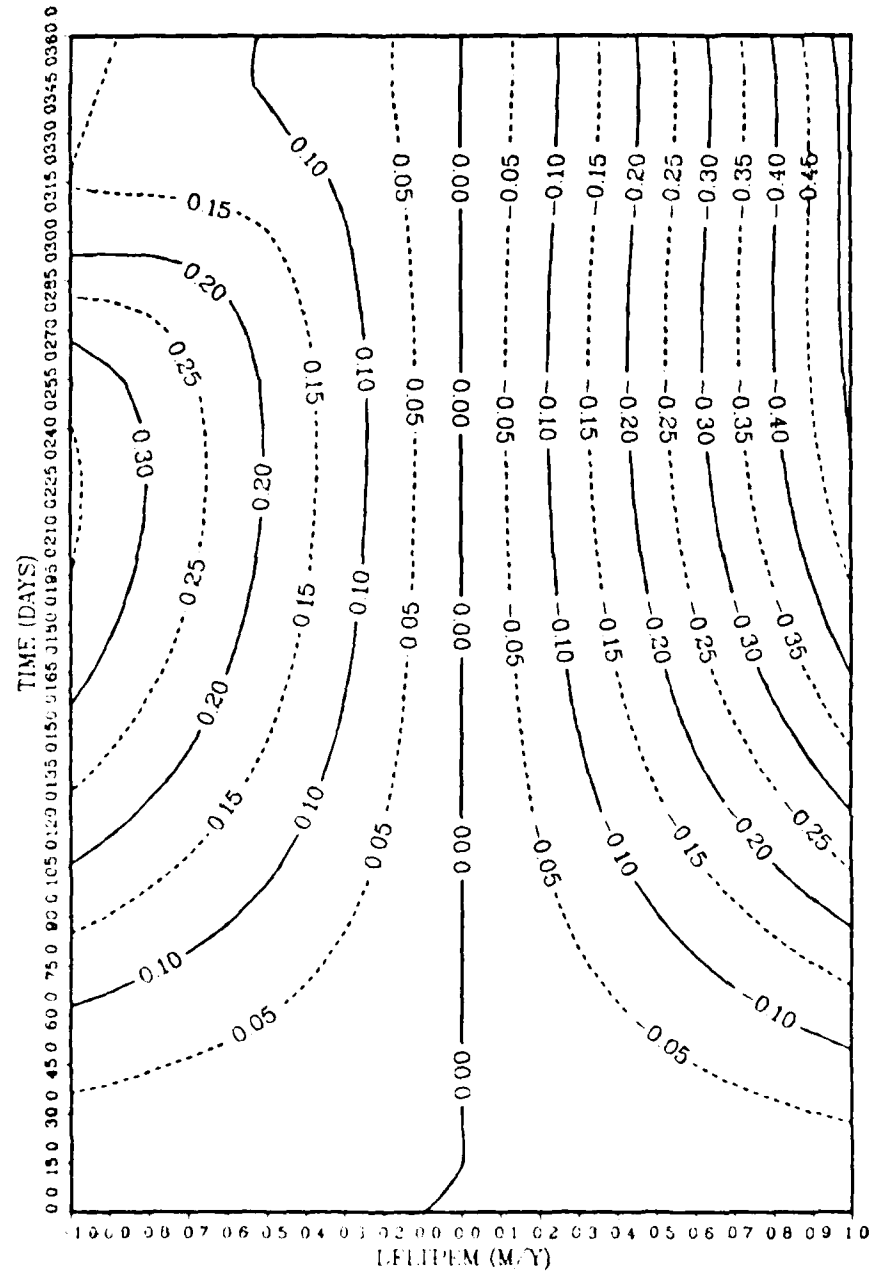Figure 3.7 Mean annual salinity (ppm).

34

Figure 3.8   Mean annual salinity anomaly (ppm).

35

Figure 3.7 depicts the mean annual salinity for the hypothetical cases studied, and Figure 3.8 depicts the mean annual salinity anomaly. From these figures, it is seen that when evaporation exceeds precipitation, the salinity is greater than the case without evaporation. With continuous evaporation, the salinity value increases. However, when the mixed layer entrains the lower salinity water from below, the salinity decreases, countering the effect of surface evaporation. From Figure 3.7 it is apparent that as the evaporation rate increases, the salinity value also increases, but then it drops. This indicates that the mixed layer depth is affected. The higher value of salinity occurs near day 220, with a value of 34.35 p.p.m. When the precipitation exceeds evaporation, the salinity is decreased by the continuous net rainfall. A striking feature in Figures 3.7 and 3.8 is the almost horizontal contour lines occurring after day 180. The reason for this is that the precipitation is providing fresh water at the same rate that entrainment is providing salty water. Hence there must exist a near-perfect balance between the surface and entrainment salinity fluxes for almost the entire last half of the year.

Figure 3.9 depicts the mean annual temperature for the cases studied, and Figure 3.10 shows the mean annual temperature anomaly. These figures show that starting with an initial temperature of $5.48\,^{\circ}C$, the surface water gets warmer with either net precipitation or net evaporation. A peak temperature value of approximately $14.5\,^{\circ}C$ at day 165 to day 175 was obtained for P-E = 1 m year, after which cooling occurred throughout the rest of the year, returning to a value near the initial one. This shows a marked annual cycle. As expected, the water warms during April through September (day 180), corresponding to the heating period. The water cools during the remaining period. The maximum temperature is associated with the late summer or early autumn, and the minimum value with the late winter or early spring.

For the case of net evaporation the mixed layer is deeper, causing the heat to be concentrated over a greater depth and reducing the seasonal temperature increase. However, the fall cooling rate is less than the cooling rate when net precipitation is considered. This feature can be related to the annual cycles of heating and cooling and of typical temperature profiles at Ocean Station "P". In April (as shown in Figure 3.9 corresponding to days 15-30) with the advent of the heating period, a thermocline is formed. The overlying waters continue to warm, and the thermocline grows until the end of the heating period. The heat is not transferred below the thermocline, and a
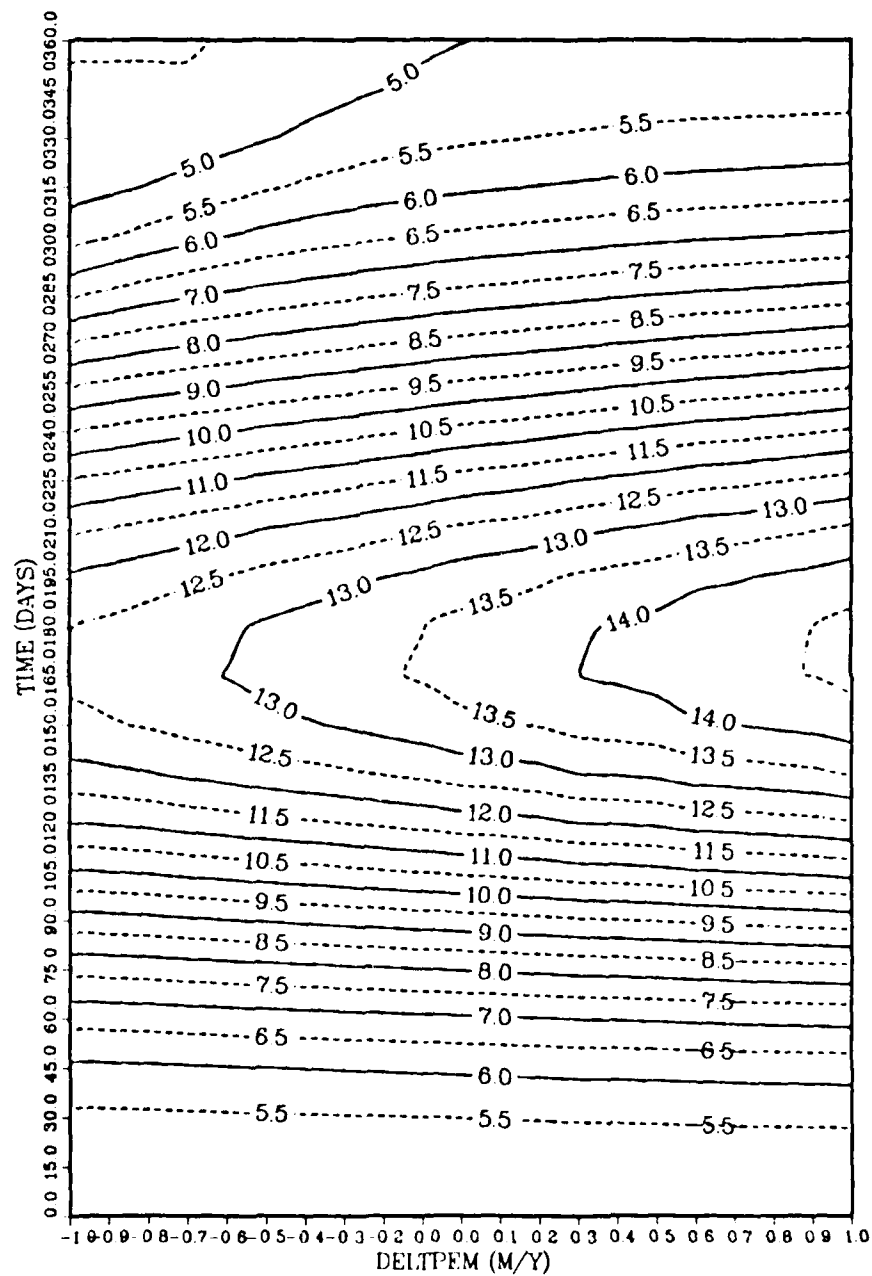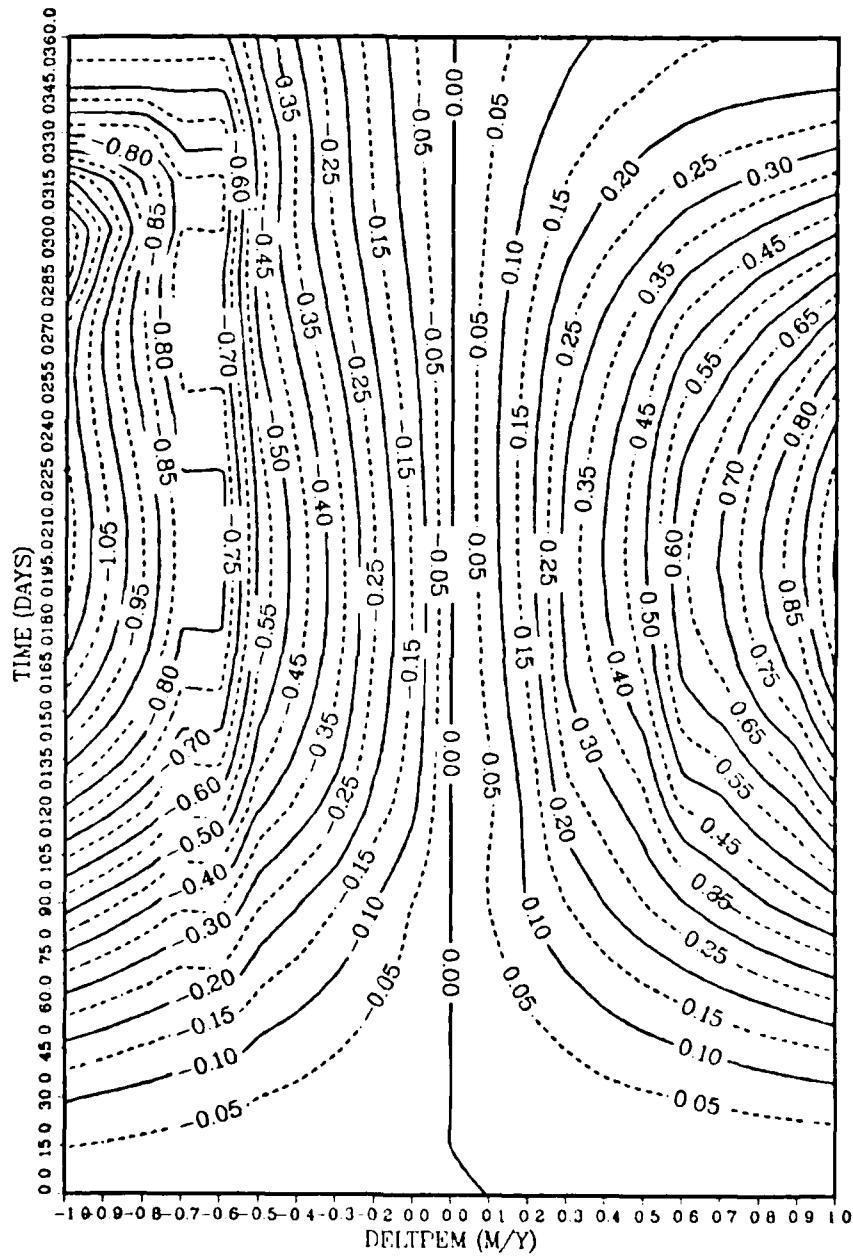
Figure 3.9   Mean annual temperature (°C).

37

Figure 3.10 Mean annual temperature anomaly (°C).

38

remnant of the cold isothermal (isohaline) structure formed during the previous winter remains. During the cooling period, the surface layer cools and deepens. The thermocline decays and sinks. Usually by March it vanishes along with the secondary halocline. The heating is due mainly to radiant energy from the sun which occurs only during daytime. During the heating period some of the heat gained in daytime is retained through the night; hence there is a cumulative heat gain. Between day 120 and day 180 (beginning of the cooling season), cooling and evaporation become dominant. The density of the surface waters increases and convective mixing occurs. This process erodes the thermocline gradually throughout the cooling season (Dodimed, Favorite, Hirano 1962) [Ref. 9].

Figure 3.10 shows the evolution of the seasonal temperature anomaly. The anomaly value increases with the amount of precipitation and also with time to a peak value of approximately $1^{\circ}C$ at day 195 (beginning of October). This coincides with the minimum low salinity value (33.5 ppm), and a shallower mixed layer depth.

C.   SUMMARY OF SENSITIVITY STUDY

It is clear that a net value of precipitation or evaporation may have a significant effect on the seasonal cycle of the mixed layer. The freshwater flux across the air-sea boundary is likely to affect the salinity field in the upper zone. The freshwater flux is determined mainly by the incoming fresh water due to precipitation and the outgoing fresh water due to evaporation (P-E). The surface water of the ocean becomes diluted or concentrated, depending on wether or not fresh water is added or taken away. Dilution in the open ocean is mainly accomplished by precipitation. Salinity concentration on the other hand, is accomplished by evaporation of fresh water from the sea surface.

It is concluded that net precipitation or net evaporation or P-E have a potentially large effect on the mixed layer, but the effect is not significant unless there is an accumulation of net P-E over time.

IV. ANNUAL SIMULATION AT OCEAN STATION "P"

Since the OPBL model depends on the interaction between the heat and momentum fluxes to determine the amount of TKE available for changing the mixed layer depth (MLD), it is important that the phase and magnitude of the surface wind forcing and surface heating be represented realistically by the forcing data used for the model boundary conditions. It is also important to provide realistic initial conditions for the thermocline and halocline below the mixed layer. The steepness of the pycnocline will determine the rate of deepening of the mixed layer by a given amount of available TKE.

A. OCEANOGRAPHY AND METEOROLOGY OF THE REGION

Since 1949 the waters of the northeast Pacific Ocean region have been surveyed oceanographically year-around. This includes oceanographic observations at Ocean Weather Station (OWS) "P" (Lat. 50°N, Long. 145°W). The available data reveals many features of the temporal variations of the water properties at this position. Furthermore, the year-around continuity of the data collection at OWS "P" enables analysis of the sequence of oceanographic events that have occured in the region between the periods of the major surveys (Susumu Tabata 1961, Susumu Tabata 1965) [Ref. 10] [Ref. 11].

The North Pacific Ocean is dominated by a low pressure system (Aleutian Low) in the winter and by a high pressure system (North Pacific High) in the summer. During October through April, the core of the Aleutian Low lies generally along the Aleutian chain, from the Kamchatka Peninsula to the Alaska mainland. The North Pacific High, on the other hand, lies generally about 2000 km west of the Pacific coast of the United States and is present from May through September. These two systems govern prevailing mean surface winds in the northeast Pacific. During the winter, the Aleutian Low results in the mean air flow being directed northward in the Gulf of Alaska. In the summer, the North Pacific High causes winds to be directed to the southeast or east. At Station "P" the prevailing winds are southwesterlies for all seasons. Although the direction of the mean monthly winds does not change much from season to season, the magnitudes of winds are about twice as large in winter (13 m s) as in summer (Meteorological Branch 1961) [Ref. 12].

Under the influence of the wind system over the North Pacific Ocean, the surface waters flow eastward across the North Pacific. Station "P" lies in the path of this flow. This flow consists of the West Wind Drift and the Subartic Current. The former carries the mixed water of the Kuroshio and the Oyashio, and the latter transports the Oyashio water that has not actively mixed with the Kuroshio. In the vicinity of Station "P" these two currents are not easily distinguishable, and the Station appears to lie in the vicinity of the boundary between these two currents.

The dominant features of the salinity structure of the Eastern Subartic Water in the region are the presence of an upper zone (0-100 m), a halocline (100-200 m), and a lower zone (> 200 m). The upper zone is characterized by relatively low salinity water (32.7 ppm). In winter, the water in this zone is mixed to homogeneity, and hence the salinity in the zone is considered constant. However, in the summer an appreciable vertical salinity gradient is present in the zone. The halocline represents a transitional zone between the upper and lower zones. Here the salinity increases with depth by as much as 1.0 ppm over an interval of only 100 m. In the lower zone, the salinity increases gradually with depth.

The water in the upper zone is isothermal in winter. However, in the summer a well defined thermocline occurs in this zone, and the temperature may decrease with depth by as much as $8°C$ over an interval of only 20 m. In the halocline the temperature generally decreases with depth. Occasionally a temperature inversion may occur, accompanied by a compensating downward salinity gradient. In the lower zone the temperature decreases gradually with depth.

To the south of the Subartic Water lies the Subtropic Water. The Subartic Boundary separates these two water masses. The boundary lies about 400 miles south of Station "P". The Subtropic Water is more saline and warmer than the Subartic Water. It has been shown (Tully and Dodimead, 1957; Dodimead, 1958) [Ref. 13] [Ref. 14] that the Subtropic Water lacks the characteristic halocline of the Subartic Water and posesses a salinity minimum at depths ranging from 200 to 600 m. Furthermore, the Subtropic Water has no major temperature inversion.

Northwest of Station "P" lies the "dome". It is characterized by relatively higher salinity and lower temperature than is present in the immediate surroundings of Station "P".

1. Factors affecting the variability of temperature and salinity

The net heat flux across the air-sea boundary is composed of two principal fluxes radiation and the turbulent heat flux. The radiative heat flux represents the combined effects of incident solar radiation, reflected solar radiation, and effective back long-wave radiation. The turbulent heat flux consists of latent heat by evaporation and conduction of sensible heat. While the radiative flux can be estimated with a reasonable degree of accuracy the same is not necessarily true for the turbulent flux. The net heat flux has a pronounced annual cycle with the maximum heat gain occurring in summer and maximum loss occurring in winter.

The freshwater flux across the air-sea boundary affects the salinity field as the heat flux affects the temperature field. The freshwater flux is determined mainly by incoming freshwater from precipitation and by outgoing fresh water from evaporation. This flux is computed in this study using observed precipitation amounts and calculated evaporation rates. Both precipitation and evaporation undergo annual variations, reaching their respective maximum and minimum at about the same time in November of each year.

B. SIMULATION OF MIXED-LAYER THERMO-HALINE RESPONSE AT OWS "P"

The data from Ocean Weather Station (OWS) "P" consist of 3-hourly surface meteorological and regular (2 - 4 times day) subsurface BT measurements during 1967. The 3-hourly forcing that can be derived from the surface observations at OWS "P" resolves very well the local diurnal and synoptic meteorological fluctuations and hence the diurnal and synoptic-scale responses for the model.

The first part of this numerical experiment, using realistic forcing, consists of running the model with no surface fresh water flux (no precipitation or evaporation), and then running the model with a hypothetical constant (annual average) value for precipitation minus evaporation (P-E). The purpose is to determine the sensitivity of the model to net P-E over a seasonal time period and longer. A number of model integrations were made, changing each time the value of P-E (in steps of 0.1 m year). Two of these runs are shown here.

Figure 4.1 depicts observed and calculated values of MLD at OWS "P" for 1967 for the null case with P-E = 0 m year. Figure 4.2 shows the results at OWS "P" for 1967 for the case of most representative P-E = 0.5 m year, most representative of the P-E mean at OWS "P".
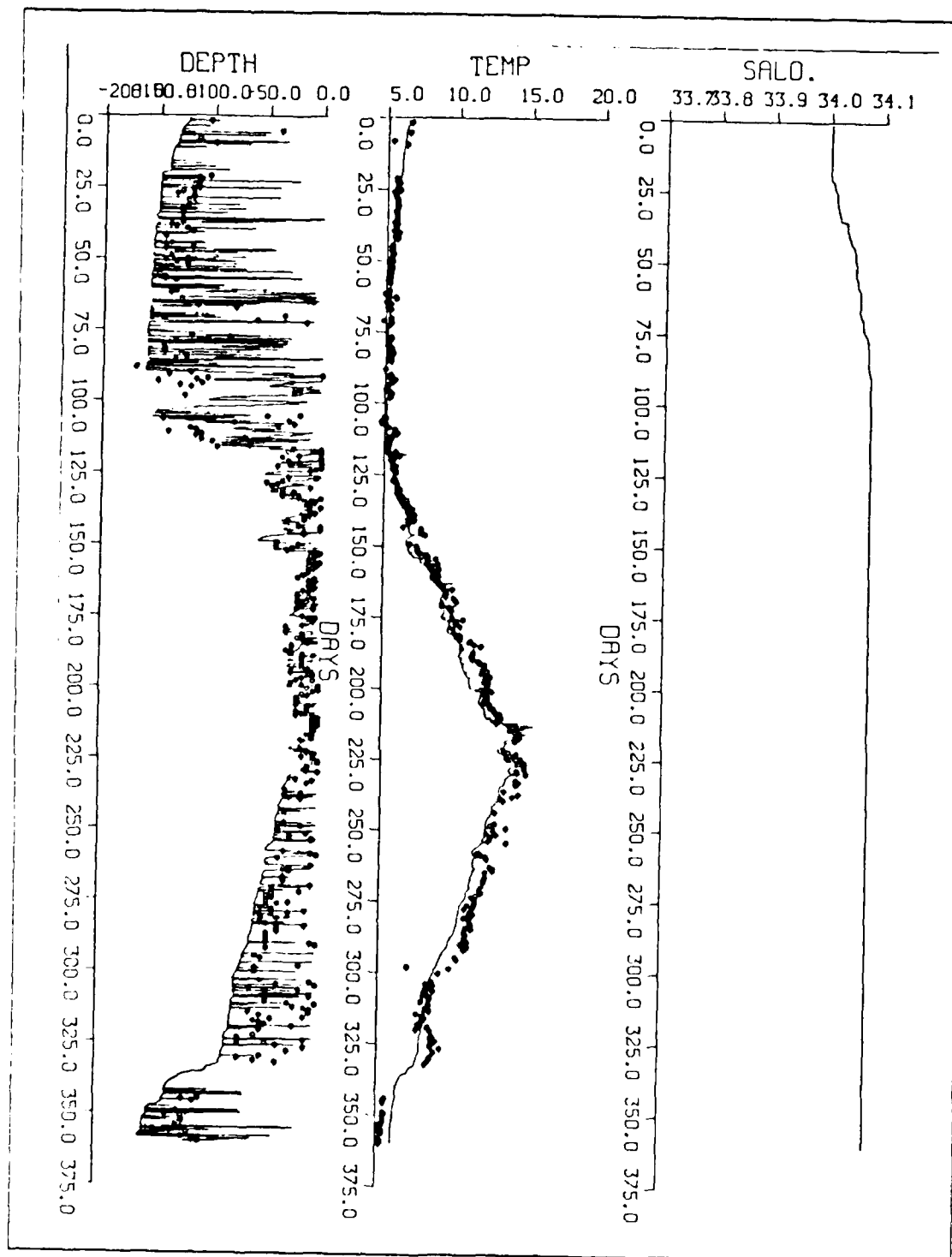
Figure 4.1   Observed (dots) and simulated SST, MLD
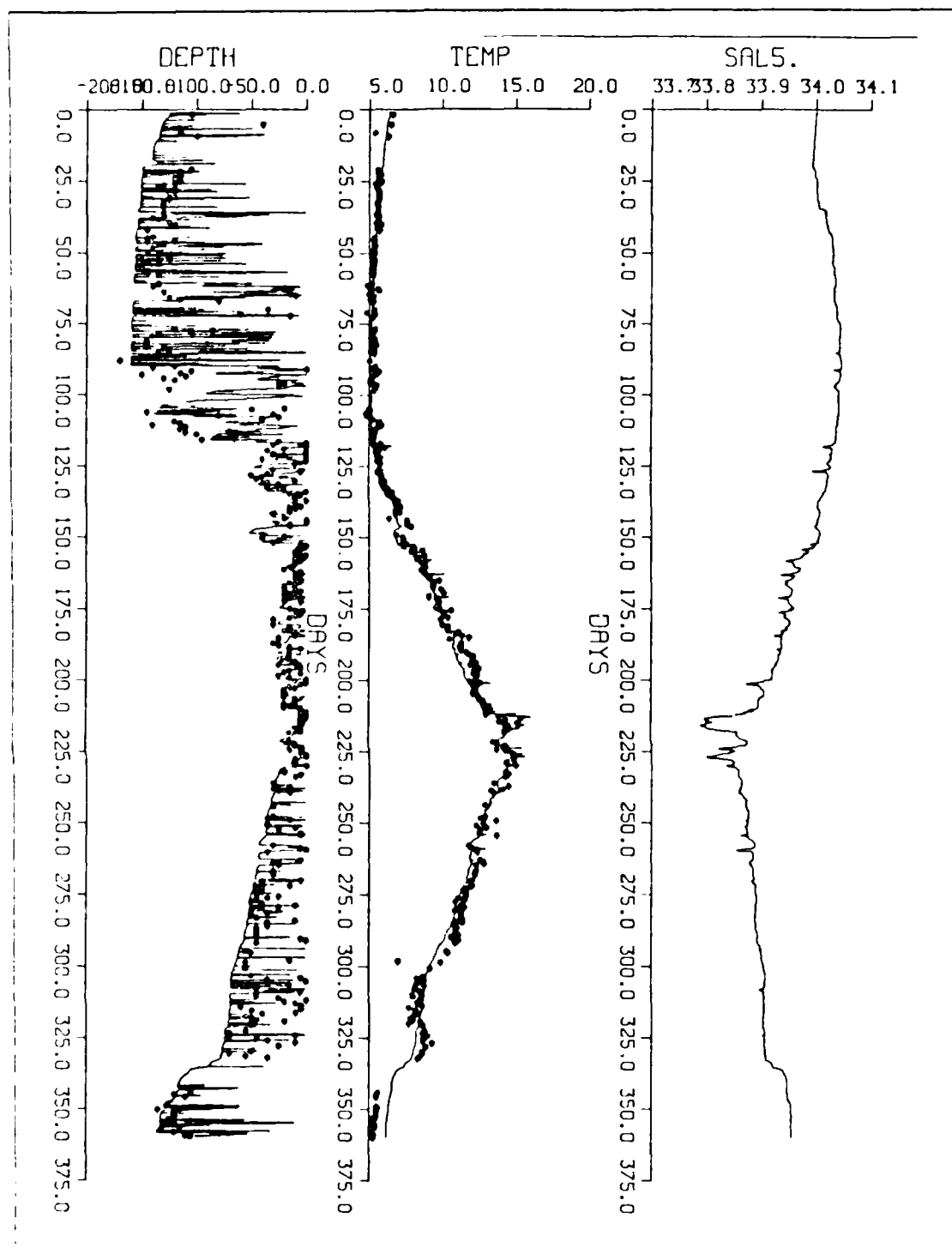and salinity (P-E = 0).

43

Figure 4.2 Observed (dots) and simulated SST, MLD and
salinity using a constant P-E = .5 m year.

From Figure 4.1 it is apparent that the MLD is too deep at the end of the year with the absence of P-E. With the addition of small values of P-E (order of 0.1 m year) there is no significant improvement in the MLD and temperature prediction. However, as more precipitation is added, the MLD becomes shallower and shallower.

The climatological monthly values of precipitation (Table 1) show that it rains much more during the fall than does during the rest of the year. Therefore, this season is expected to be particularly important for this study. As shown in Figure 4.2, starting at about day 270, the first day of fall, the observed MLD is about 40 meters. Also shown is an apparent peak in MLD at the end of the year which is too shallow in comparison to the observations. This means that perhaps there is another process that is important that is not included here. Salinity between days 0 and 100 shows a small increase because the mixed layer is deepening. By deepening, it is entraining higher salinity water from below with a greater influx of salinity than can be compensated for by precipitation. In the spring, the salinity falls until late summer when it rises again when the mixed layer resumes deepening. From this it is apparent that there needs to be more rain in the fall season than during the rest of the year. Overall, this series of hypothetical constant P-E runs shows that sufficiently strong precipitation can counter the fall and winter effect of too-large a predicted deepening rate. This tends to verify the hypothesis that seasonal-scale forcing has a similar effect as the smooth-forcing case first studied.

To create more realistic values for P-E, average monthly values of precipitation are taken from Dorman and Bourke (1979) [Ref. 8]. Table 1 shows the average monthly values of precipitation at Ocean Weather Station "P". These values will be included in the model in 30 day steps, thus providing a realistic if not precise seasonal variability to the salinity forcing. Summing these values indicates an annual precipitation rate slightly more than 1 m year.

For the next numerical experiment, E is set equal to zero and P is changed monthly according to the values in Table 1. Figure 4.3 shows the resulting prediction for MLD, temperature and salinity. Salinity starts at 34.0 ppm at the beginning of the year, and an almost insignificant decrease is observed through January until middle February after which salinity increases slightly until about the beginning of April. At the same time, temperature decreases to a minimum value of $5°C$. MLD generally is increasing throughout these first 100 days. This shows that the entrainment of higher salinity water from below is occurring at a faster rate than fresh water is being precipitated, even though precipitation is large for January and February.

45

TABLE 1

MONTHLY AVERAGE RAINFALL AT OCEAN STATION "P"

January	105	mm.
February	100	mm.
March	65	mm.
April	65	mm.
May	60	mm.
June	35	mm.
July	30	mm.
August	50	mm.
September	105	mm.
October	125	mm.
November	145	mm.
December	130	mm
SUM	1015	mm.

From the middle of April to the end of November, salinity falls to a value of 33.75. At the same time MLD drops and then increases steadily again from August until the end of the year. The temperature reaches a maximum value of almost $15°C$ at day 225. After this, temperature steadily decreases, with a particularly rapid decrease after day 330. The final temperature at the end of the year is slightly warmer than it was for the annual simulation using P-E = 0. The salinity after November shows a rapid increase, ending the year with a value of 33.82 ppm. The reason for this increase is the rapid entrainment of underlying water with higher salinity. Most significantly, the depth of the mixed layer is about 40 meters shallower than the case with P-E = 0. One factor preventing the MLD from being even deeper in the winter is the permanent halocline at 150 meters. Also, there is no vertical diffusion in the model, and this may influence MLD somewhat.

The next step in this study was to compute improved evaporation values using the Equation (4.1). where Q_e = evaporation heat flux [cal $(cm^2 sec)$], ρ_w = density of the ocean water (1.025 gm/cm^3), L = latent heat of evaporation (590 cal gm), E = required evaporation value (cm sec) Using equation 4.1, daily values of evaporation were computed. Figure 4.4 depicts these daily average values of evaporation (cm sec) at Ocean Station "P" for the year 1967.

Generally, evaporation is greatest when there is a strong wind. In the summer the sky is expected to be relatively clear and the air relatively warm so evaporation should be expected to be relatively high. In the winter the air temperature is relatively
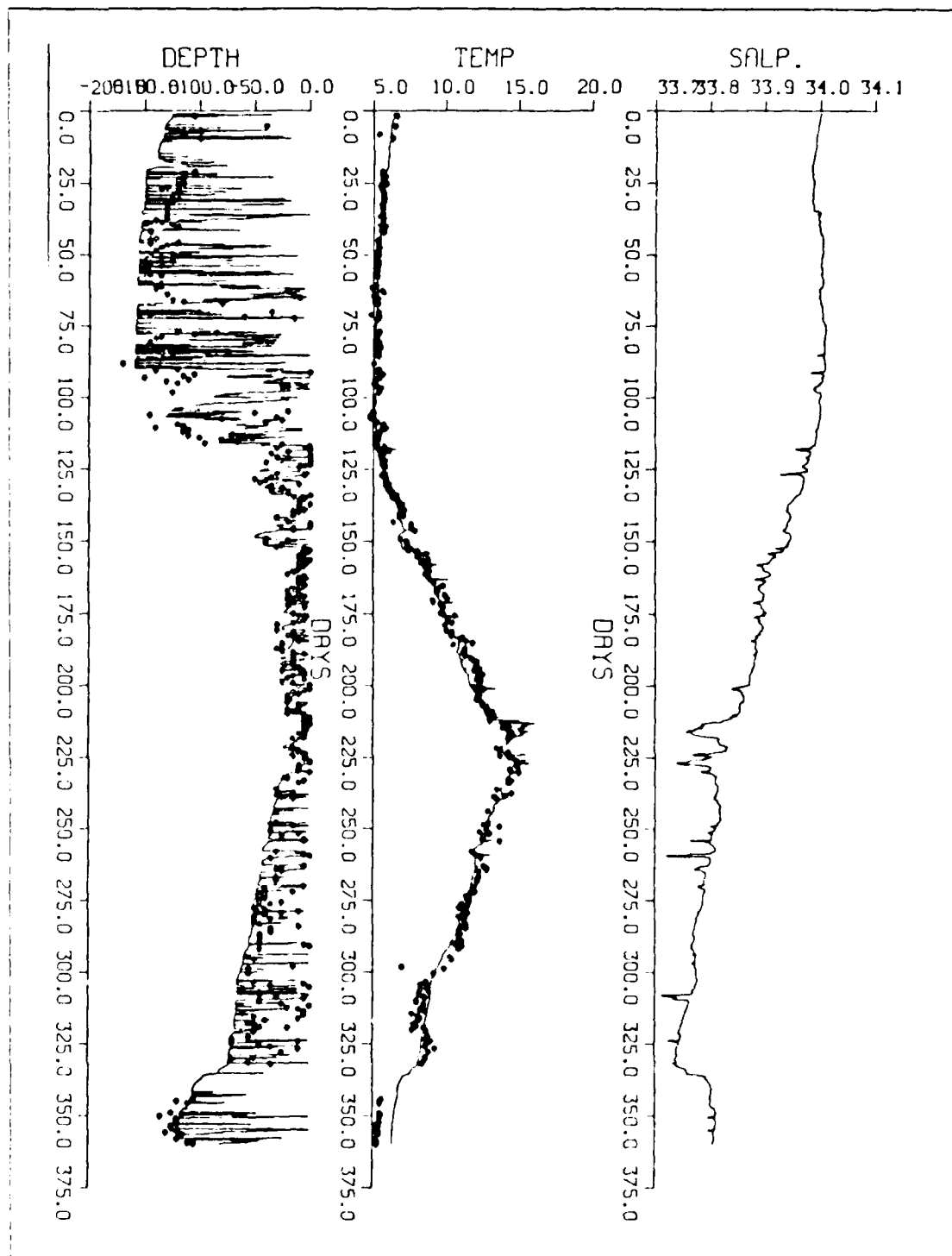
Figure 4.3   Observed (dots) and simulated SST, MLD and salinity with P
varying monthly according to Table 1, and E = 0.

$$Q_e = \rho_w L E \qquad (4.1)$$

cold and there are more clouds, but the wind speed is very high. So more evaporation can be expected because with higher wind speeds cause evaporation increases. In summer it happens that there is considerable fog at Ocean Station 'P'. This means a high relative humidity. Comparing this to Figure 4.4, higher values occur when there are high wind speeds, and the most extreme values occur when continental dry air is also present.

Fall starts at day 270, and higher rates of precipitation begin. So it is probable that rain rate will exceed evaporation considerably in this season, even though evaporation rates are large at this time. Evaporation exceeds precipitation on a monthly basis only during May and August. The rest of the year is characterized by P-E > 0. It is necessary to recognize that the calculation of evaporation is only an approximation because it does not account for the evaporation of spray. When water waves break in the presence of wind, spray is formed which is not included in the latent heat flux, but should be partially included in the evaporation calculation. Drops of salt are formed by evaporation of the spray. This salt falls back into the water, increasing the mixed layer salinity. It is not known yet how important the spray effect is. However the method of computing evaporation can be considered as a good first-order guess.

Using daily average values of evaporation together with monthly values of precipitation is a mixing of time scales, but actually daily precipitation rates are not available. Figure 4.5 shows the observed and simulated values of sea surface temperature and mixed layer depth, along with the simulated values of salinity at Station 'P' with monthly values of precipitation and those daily values of evaporation. This figure shows that starting in early summer, temperature is a little warmer than the temperature when no precipitation and no evaporation was included in the model. The temperature ends up only slightly colder than the case where just precipitation was considered. The salinity shows a small decrease at the beginning of the year, but after day 20 it starts to increase in value until April. It reaches a peak value of approximately 34.6 ppm due to the entrainment of water with higher salinity from below at a rate faster than the net precipitation. During May and September small increases in salinity are apparent due to evaporation exceeding precipitation in those two months. Salinity again increases at the end of the year due to entrainment. The
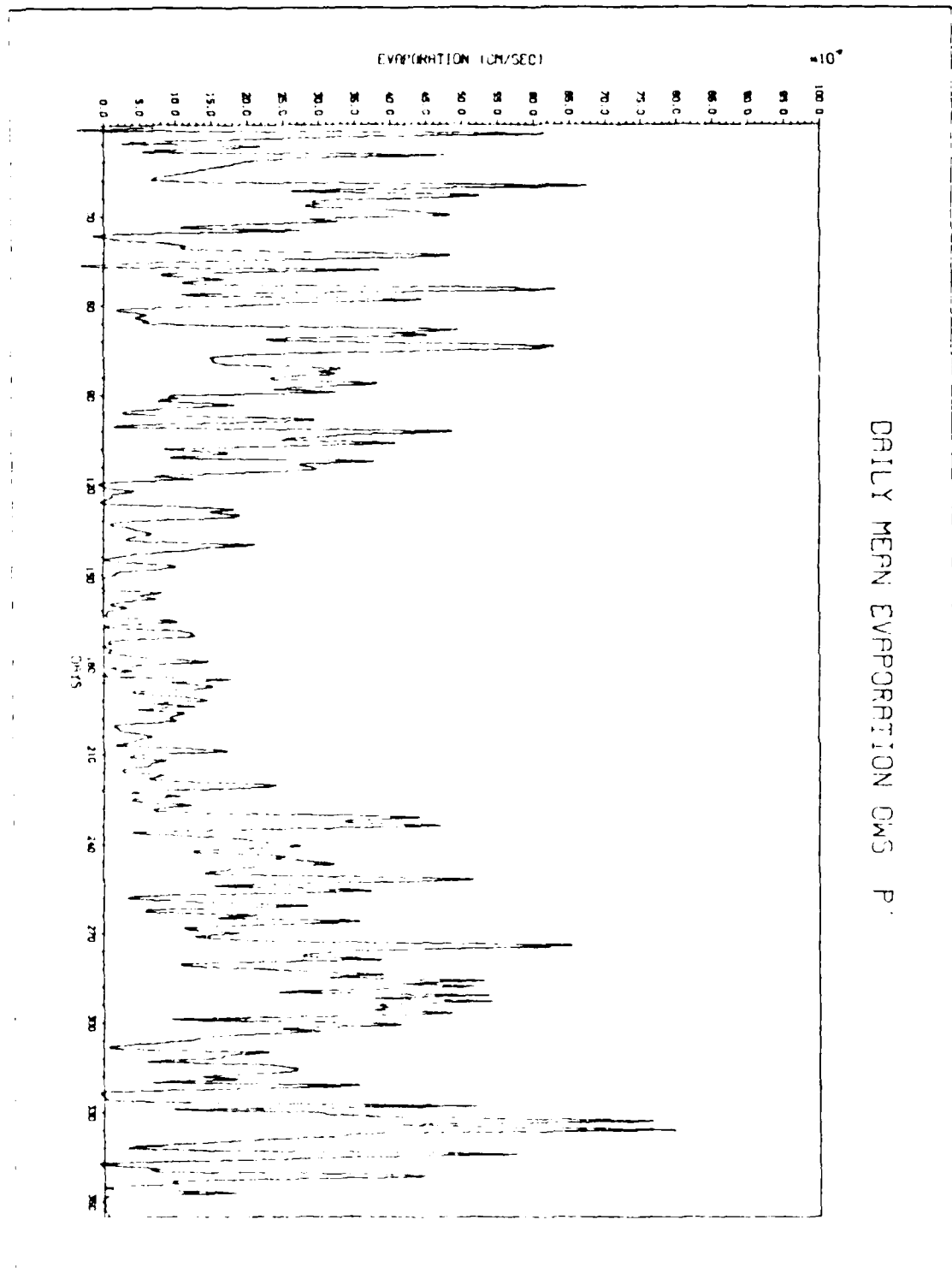
48

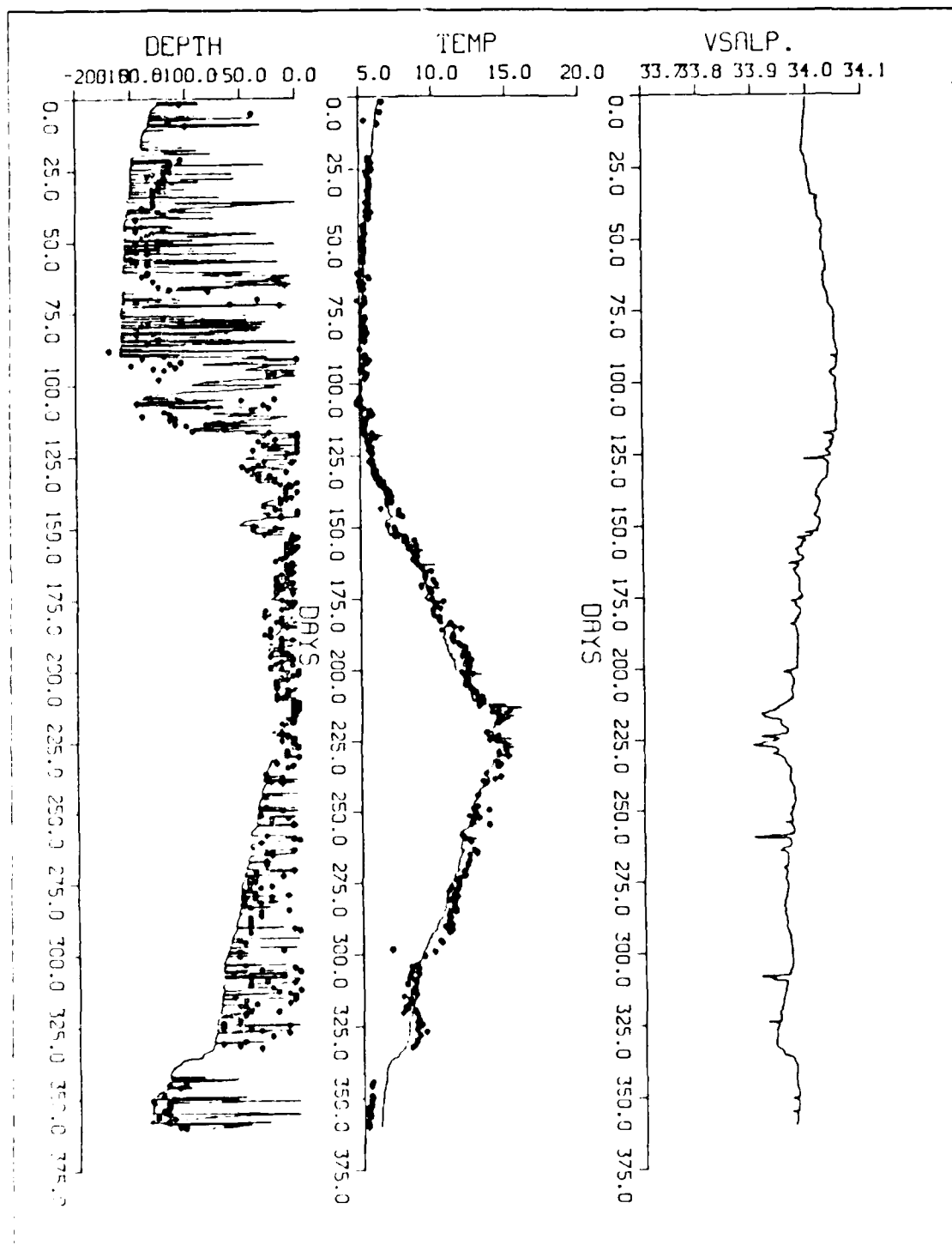Figure 4.4   Average daily values of evaporation.

Figure 4.5 Observed (dots) and simulated SST, MLD and Salinity
with monthly-varying values of P and daily values of E.

net change in salinity over a whole year is less than 0.1 ppm, but there is an important effect upon the MLD which is roughly 25 meters shallower than for the case with no freshwater flux. This 25 meters represents a 20% change in MLD. From the predicted MLD, it is clear that the difference begins in the early spring at which time the mixed layer forced begins to shallow. There is a net accumulation of about 57 cm of water. After one year, net precipitation minus evaporation is about 49 cm. This value is very close to the hypothetical case for which precipitation minus evaporation was set equal to a constant value of 50 cm year, yielding a shallower MLD by about 20 meters after one year. Therefore, the seasonal cycle in precipitation and evaporation results in only a small final difference in comparison with the constant P-E case.

In order to observe more closely the variability in temperature and in MLD due to the presence of salinity flux, the relative differences in these variables were computed relative to the case of P-E = 0.

Figure 4.6 depicts the time series of the differences of salinity, temperature and mixed layer depth for a realistic forcing by P-E relative to the P-E = 0 case.

Note that the average MLD sometimes is deeper. This occurs occasionally whenever P-E < 0 for a few days. The largest fluctuation in relative MLD are, however, related to the diurnal cycle. The diurnal cycle can be shallower or deeper, and probably ne times when it is deeper are the cases of no rainfall. Two time scales are evident. The diurnal cycle is the most obvious, but the time scale considered to be more important in this study is the seasonal one. Salinity shows a net change over a year of almost 0.1 ppm. This is only a small difference, but it has a large effect on the MLD, showing a depth difference of almost 25 meters at the end of the year. This represents an almost 20% reduction in mixed layer depth. This case shows that the MLD differences are not very significant until after the fall deepening is well underway after day 330 (end of November). At this time the MLD difference is only 7 meters shallower. There is more precipitation than evaporation all summer long, so the surface is of lower salinity than the underlying water. In winter, rain tends to reduce the salinity of the surface water. At the end of the year, the most important effect for salinity, is that the layer is entraining underlying water that has higher salinity. A single big storm from about days 330-335 entrained enough high salinity water from below to almost completely counter the mixed layer salinity reduction of about 0.1 ppm which was caused by several months of net rainfall excess over evaporation.
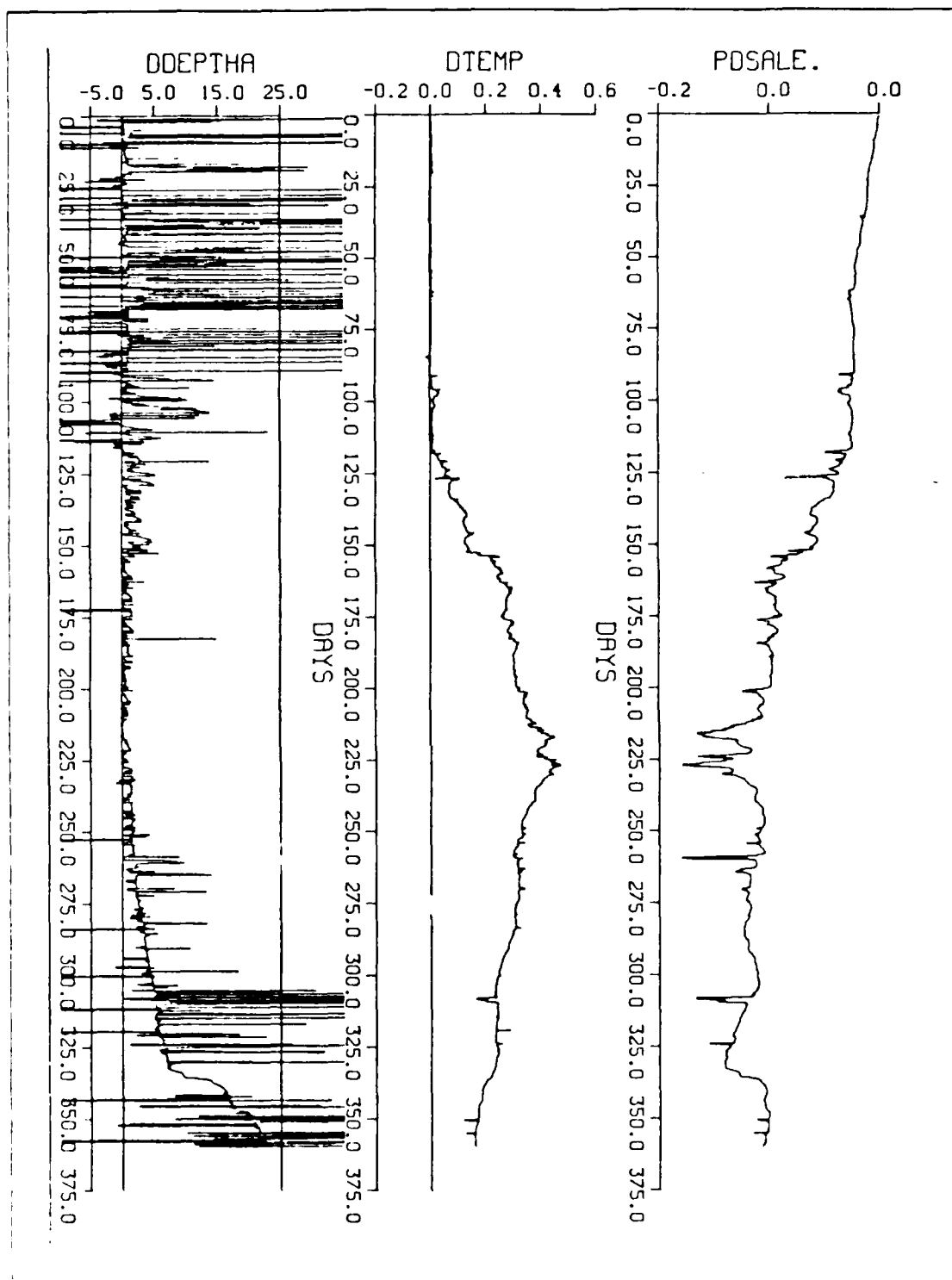
Figure 4.6 Time Series of Sal., Temp. and MLD (case w P-E - case w o P-E).

Temperature at the end of the year is half of a degree warmer than the case without rainfall. The peak temperature difference, which occurs at day 225 (summer time), is caused by the inability of spring and summer storms to mix down through the strengthening seasonal halocline. Although this happened in the shallowing season, it really is an accumulative effect of a reduction in storm mixing over several months. In Figure 4.5, at around day 148 a mixed layer temperature of $6.9°C$ is observed. This temperature falls due to a storm on about day 148. In Figure 4.6 the temperature shows an almost steady increase between days 125 and 225, and the MLD for that period of time seemed to be the same as for the P-E = 0 case. There was, therefore, no apparent reason for the temperature changes because there is no difference in heat content. A possible explanation is that heat is mixed down in a different way so it appears like that there is no significant difference in MLD. This is not obvious because most of the time throughout this period MLD was not significantly different. At times, however, the MLD spikes are different, and it is believed that this correlates with storms. For example, after the storm on day 148 where the MLD difference is about 2 or 3 meters. This mixing event occurs during the shallowing season when the mixed layer is only about 10 or 15 meters deep. Hence 2 or 3 meters for that scale represents a 15% or 20% temperature change for the same heat content. This amount of MLD difference represents a large amount of heat content if the thermocline is large. Every time that a storm occurs, only a couple of meters difference in depth results due to the added buoyancy of net precipitation, but this represents a significant difference in the vertical distribution of heat. This explains why the temperature was increasing although the MLD was usually the same throughout the period.

In Figure 4.6 it is clear that the biggest difference in temperature and salinity occurs at around day 225 which corresponds to the summer shallowing season. In order to provide more insight into the difference in vertical heat distribution at this time, vertical profiles of temperature and salinity are presented in the next two Figures. Figure 4.7 is the collection of vertical temperature profiles, once an hour, for day 225 (summer time) for the P-E = 0 simulation. Figure 4.8 represents the vertical temperature profiles, once an hour, for the same day when precipitation and evaporation values are included. Comparing Figures 4.7 and 4.8, it is apparent that the case including precipitation and evaporation is $0.5°C$ warmer than the case where no rainfall and no evaporation. This surface temperature difference is entirely due to the differences in the vertical mixing of several storms that mixed the ocean to depths of
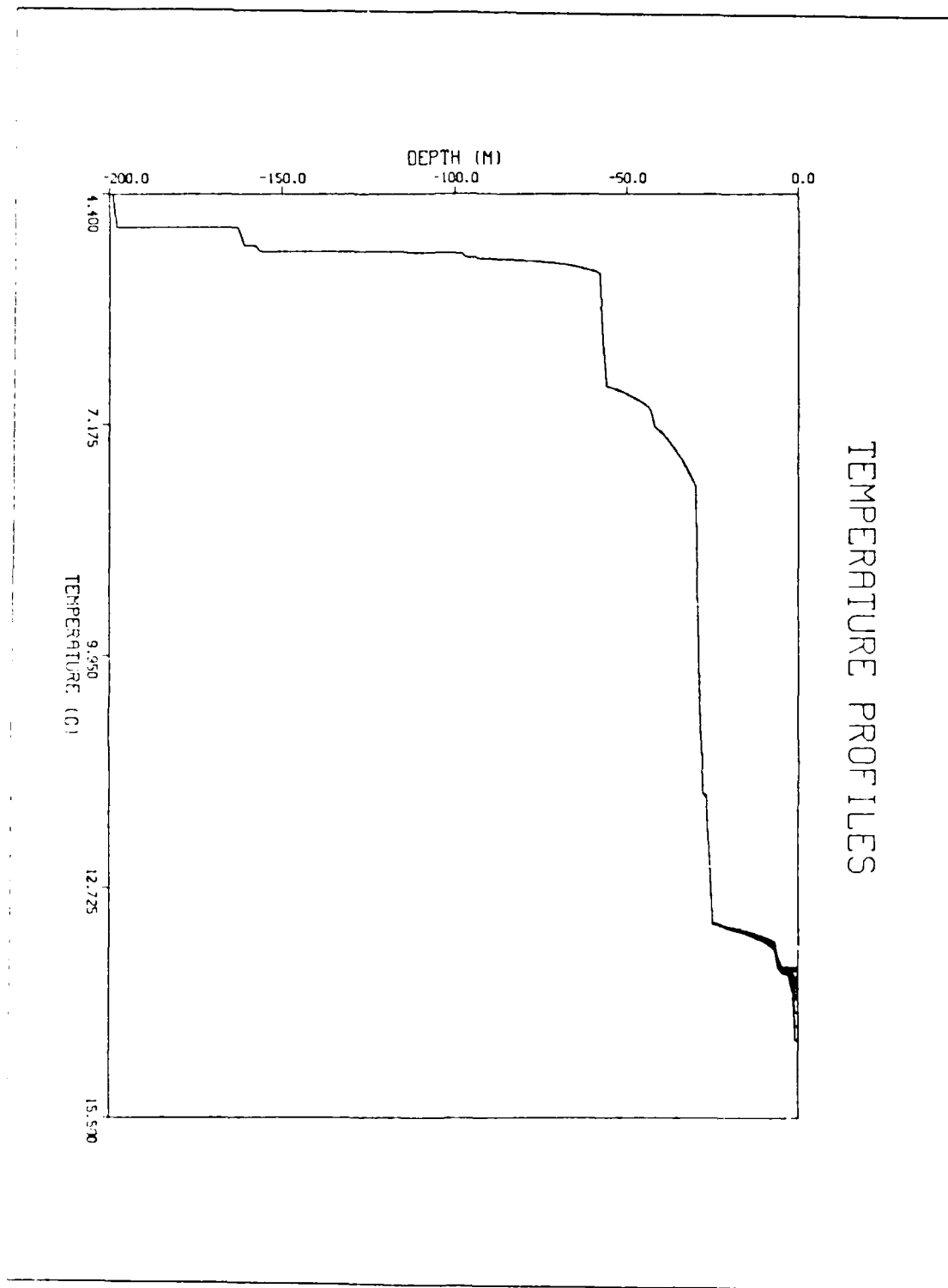
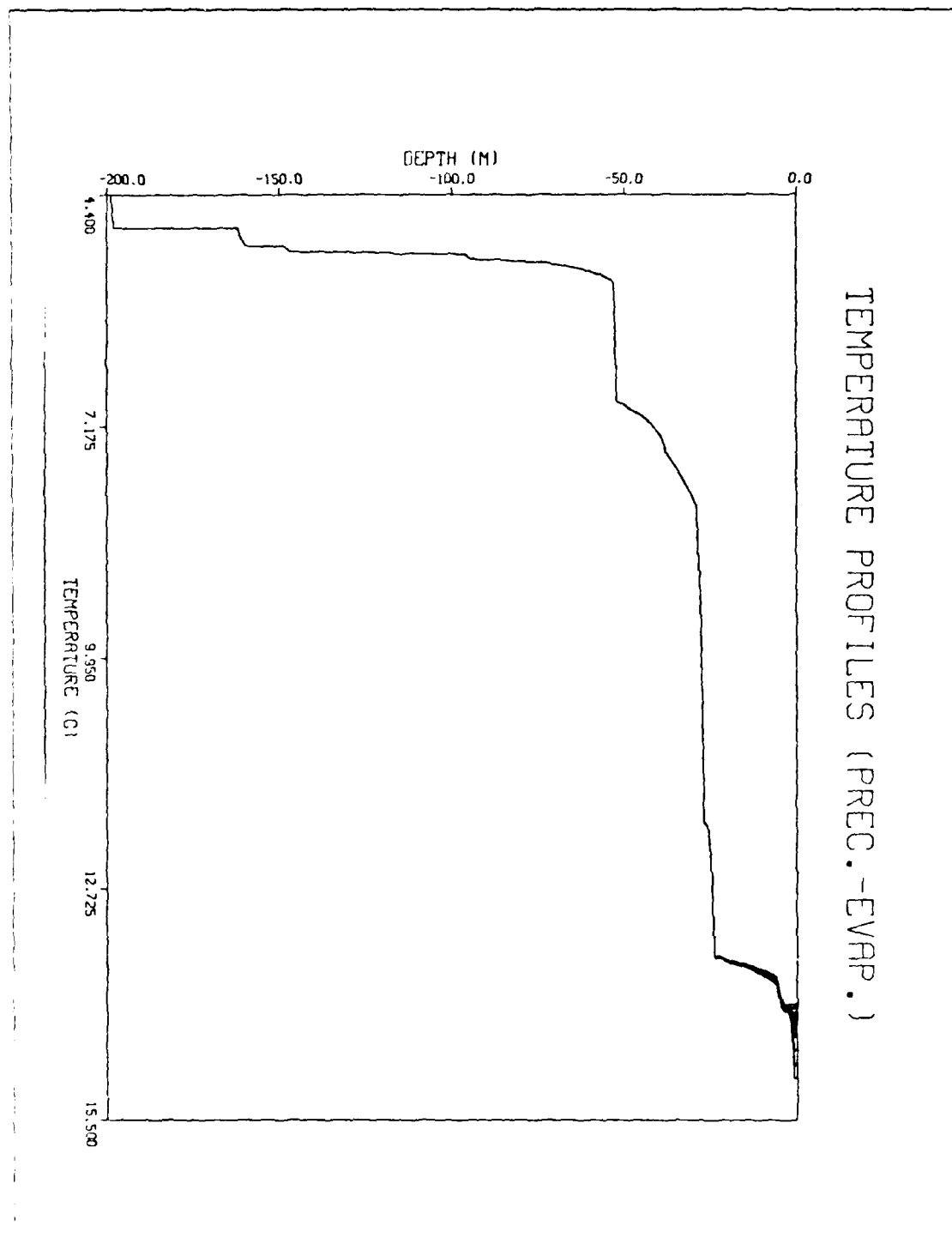Figure 4.7 Vertical Temperature profile for day 225 (P-E = 0).

54

Figure 4.8   Vertical Temperature profile for day 225
(with realistic P-E values).

55

about 55 m, 39 m and 28 m respectively. At each of these depths there are sharp thermoclines which were created in succession (Figure 4.7). These same storms mixed the ocean to the relatively shallower depths of about 51 m, 37 m and 27 m, respectively, for the simulation which included precipitation. The net heat content and the vertical integral of each of the respective profiles is of course identical. Hence the surface temperature must be reduced for the situation with deeper thermoclines.

To verify the numerical model integration, the temperature profiles were vertically integrated over the upper 200 meters for both simulations on day 225. The difference in heat content for the two cases was 0.44 °C, representing an average temperature error of only about 0.0022 °C. This small difference is attributable to computer round off error.

C.   ADJUSTMENT FOR ADVECTION OF SALINITY

Figure 4.5, shows the salinity starting value is 34.0 ppm. At the end of the year, the salinity has dropped to 33.71 ppm. This trend of about -0.3 ppm year would repeat every year (assuming the surface forcing is representative), and it must be countered in the long term by advection. In order to compensate for this trend, the linear fit (Figure 4.9) is subtracted from the predicted salinity time series to give the salinity seasonal cycle Figure 4.10. This method in essence simulates advection, and it provides a salinity time series which can be better compared with the seasonal climatology, Figure 4.10.

As was expected and because the trend was subtracted the last value of the salinity anomaly is the same value as the first point. In this way values of salinity beginning in January and ending in December must be the same. In Figure 4.10, the climatology for surface salinity shows an annual cycle with a maximum value of 0.66 ppm at around day 100 which, in late winter. There are several minima due to the transient nature of the mixed layer salinity during the summer and fall. Comparing the times at which these minima occur with the mixed layer depth plot, they are found to correspond to times when the mixed layer is most shallow.

Because no salinity data was available in adequate synoptic detail for 1967, the calculated simulation of salinity can be compared only with the climatology at Station "P" for 25 years (August 1956 to June 1981). Figure 4.11 depicts the climatology of seasonal temperature structure at Ocean Station "P", and Figure 4.12 shows the climatology for the salinity structure. From Figure 4.11 it is apparent that significant changes occur in the upper 100 meters. The surface temperature at the beginning of the
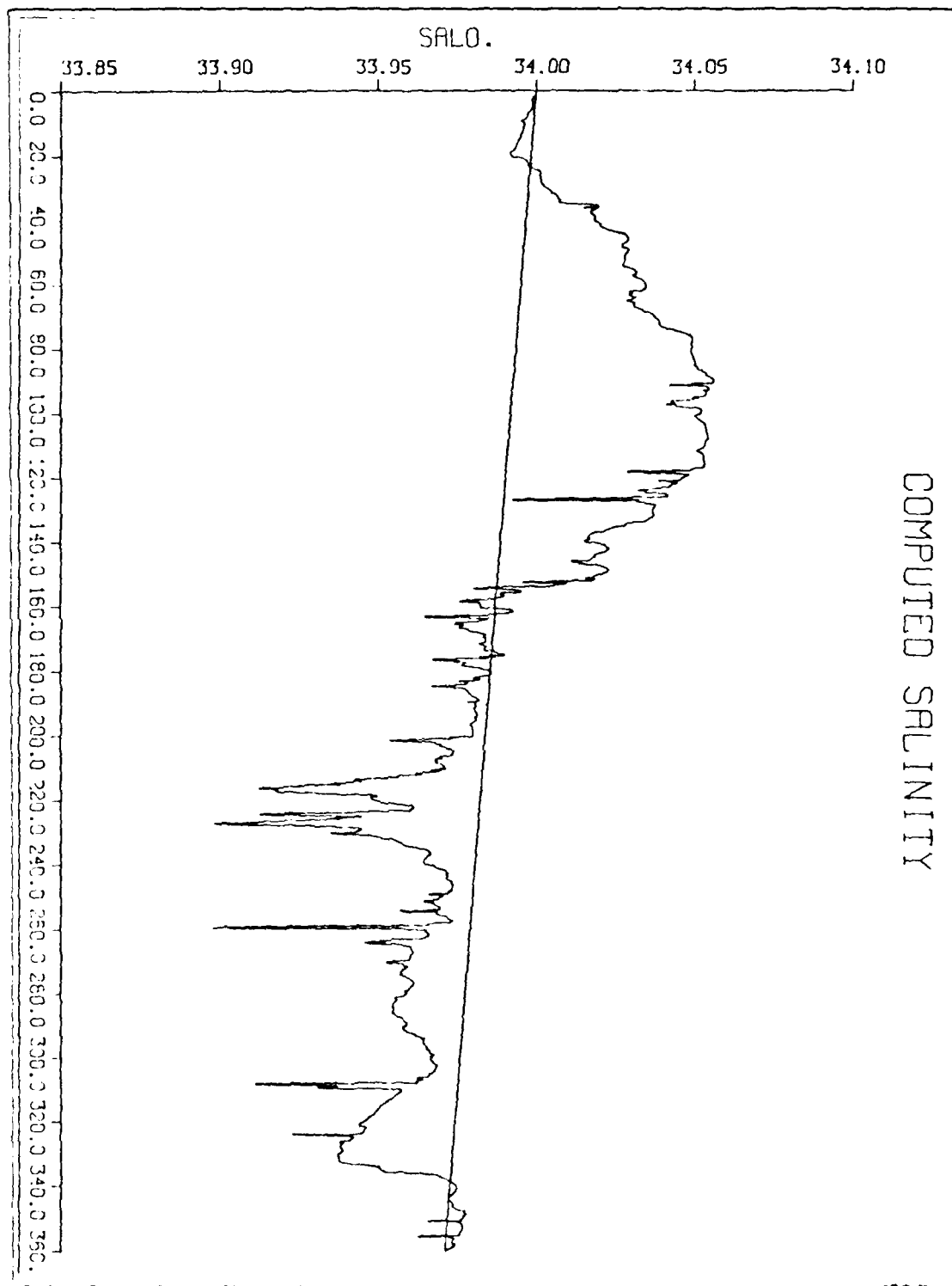
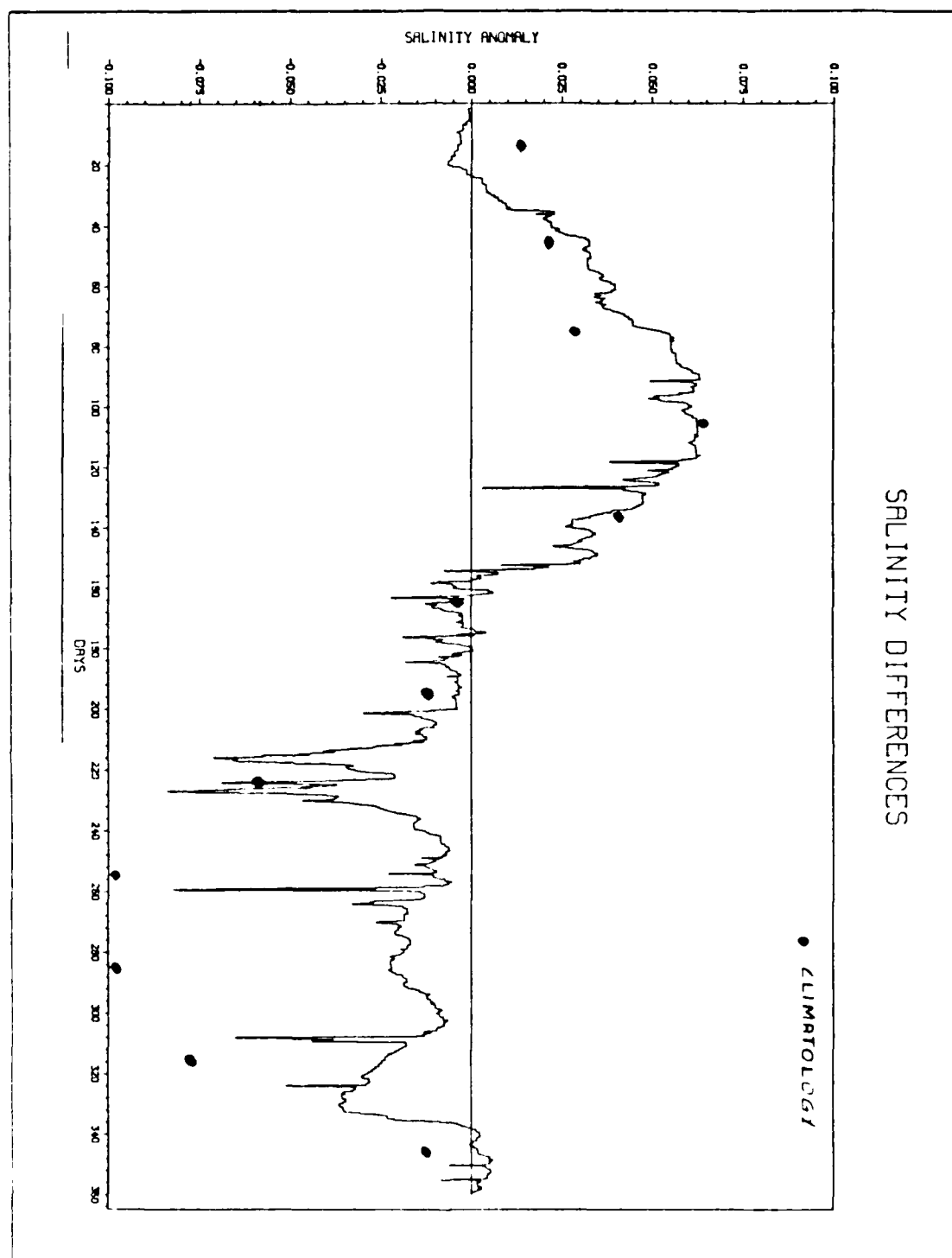Figure 4.9   Predicted salinity and Trend in Salinity for 1967.

Figure 4.10   Comparison between climatological monthly changes
in S and de-trended changes in predicted S.
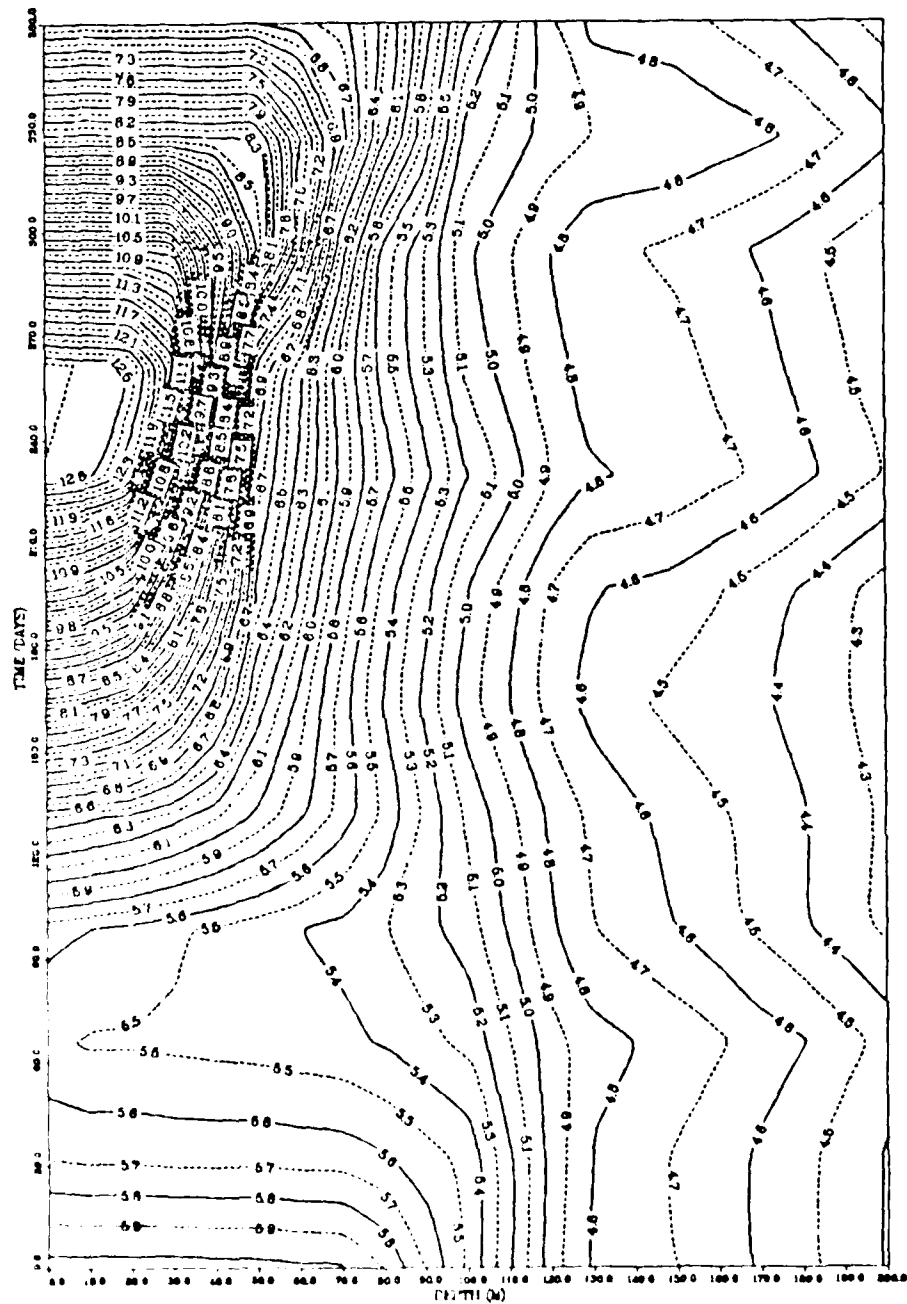
58

TEMPERATURE (CLIMATOLOGY)

Figure 4-11 Climatology of Temperature Structure at Ocean Station "P".
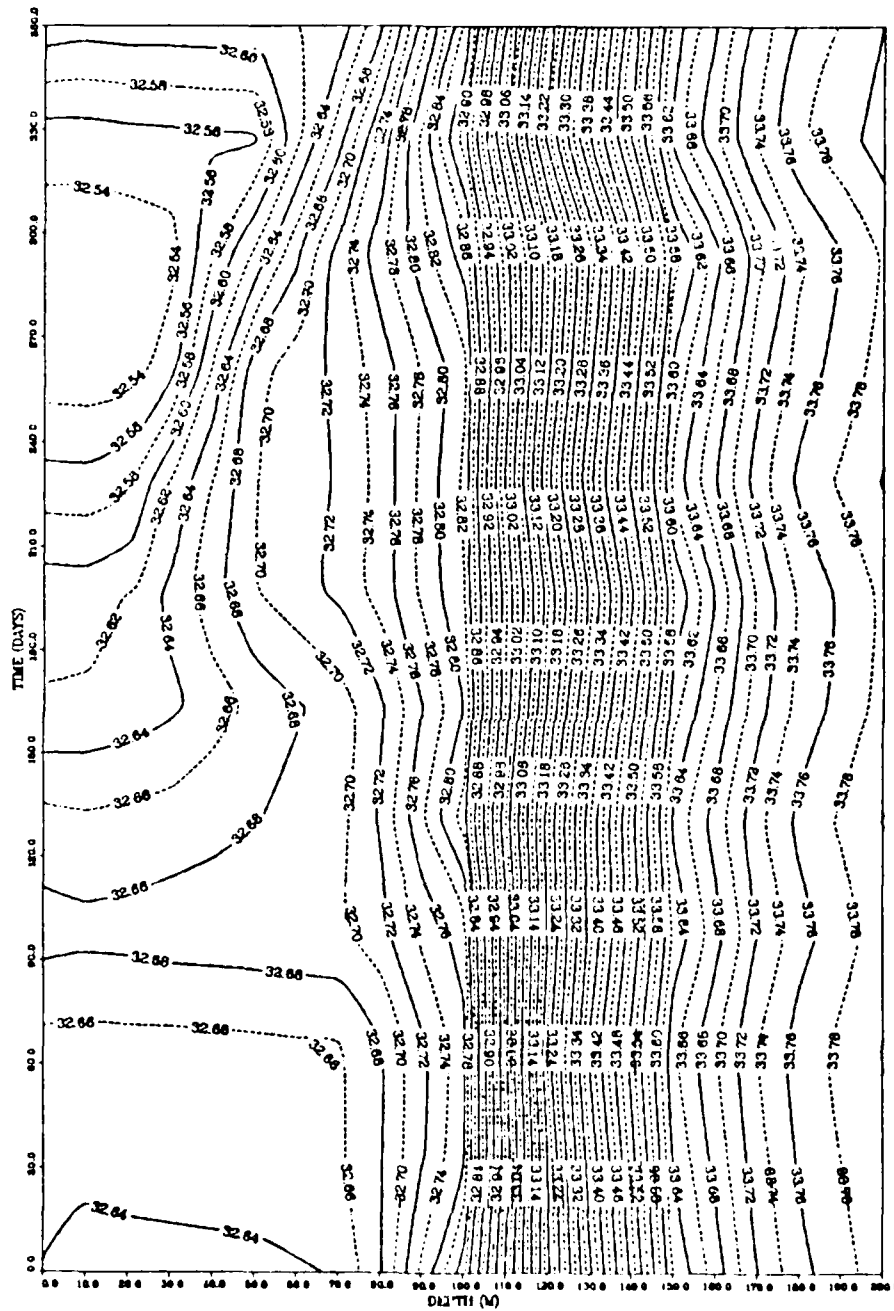
SALINITY (CLIMATOLOGY)

Figure 4.12   Climatology of Salinity Structure at Ocean Station "P".

60

year is 6.04°C. Then it cools for the next three months, reaching a minimum in March with a surface value of 5.52°C. The surface temperature subsequently warms, reaching a maximum in September with a value of 12.74°C. For the rest of the year, surface temperature steadily drops to a value of 6.80°C by December. This cycle influences the upper 100 meters. Between 100 and 125 meters, there are no significant changes in temperature over the year. Below 125 meters large changes in temperature must be due to seasonal advection of the thermocline caused possibly by seasonal-scale Ekman Pumping. In about May the apparent rise of the permanent thermocline might be due to Ekman Suction by the climatological low pressure in this region at this time of the year.

Figure 4.12 shows that salinity has a parallel seasonal structure to temperature. The surface salinity value in January is 32.64 ppm and remains almost constant for the first two months down to a depth of approximately 70 meters. In March salinity increases, reaching a maximum surface value in April of 32.689 ppm, after which salinity decreases throughout the rest of the year. It is apparent from Figure 4.12 that salinity has an almost constant value between the surface and the upper 30 meters, below which there are little vertical changes until a depth of approximately 100 meters. The almost horizontal contours in Figure 4.12 between the depths of 100 and 150 meters are due to the linear interpolation of the climatological data by the contouring routine. Below 150 meters salinity does not show evidence of Ekman pumping/suction. However, this may be due the lack of observations.

Figures 4.11 and 4.12 show that the deepest mixed layer depth is about 100 meters. However the "true" climatological deepest MLD is probably considerably greater than 100 meters. The apparent MLD in Figures 4.11 and 4.12 will be reduced by the averaging process used to construct the respective climatologes.

The climatology of surface salinity shows a big increase in April and a big drop in August through September. The biggest differences between climatology and the single year prediction of salinity (Figure 4.10) is from August until December. This climatology of Dorman and Bourke [Ref. 8] is not necessarily representative of the year in question, 1967, and horizontal advection is not explicitly included in the calculation here. Nevertheless the predicted seasonal response in surface salinity is consistent with the climatology, within expected statistical variations. In particular, the phase of the climatology signal is in agreement with the phase of the signal that was predicted.

61

V. SUMMARY AND CONCLUSIONS

The purpose of this study was to determine the effects of salinity on the seasonal-scale evolution of the mid-latitude oceanic planetary boundary layer. It was hypothesized that important aspects of the seasonal thermocline formation and erosion could only be explained by the addition of a salinity flux at the surface of a thermodynamic mixed layer model. Because of the lack of useable synoptic data for precipitation, the problem was approached in two ways: 1) using hypothetical values of precipitation and evaporation, and 2) using realistic thermal forcing and wind stress data together with climatology for precipitation.

For the hypothetical forcing case, evaporation and precipitation were assumed first to be in balance over a year to simulate an annual cycle in temperature, salinity and mixed layer depth (MLD) with no surface salinity flux. Hypothetical values of evaporation and precipitation were then specified to find the seasonal effects of a steady fresh water flux on the salinity structure and consequently on the MLD and thermal structure. For cases in which evaporation exceeds precipitation, the mixed layer salinity increases at first then decreases. Steady precipitation causes the MLD to be shallower during the whole year, but the shallowing is greatest at the end of the year due to the accumulative effect of net precipitation. For the case of steady net evaporation, the mixed layer salinity increases, but the layer entrains more water with lower salinity from below which tends to cancel the salinity increase caused by evaporation. After the first three months of net evaporation, the MLD difference grows rapidly. The upward buoyancy flux caused by net evaporation increases the turbulent kinetic energy, further increasing the entrainment rate until the spring, after which shallowing occurs. The mixed layer temperature shows a slower seasonal rate of increase when compared with the case in which precipitation is greater than evaporation.

When precipitation exceeds evaporation, the mixed layer after the third month shows a slower deepening rate, entraining water with a higher salinity. However, the dilution effect is not as great as for the net evaporation case. During the second half of the year, precipitation and entrainment of high-salinity water almost balance, causing mixed layer salinity to be almost steady for the last several months from late summer until early winter.

A series of hypothetical tests showed that precipitation and evaporation have a significant effect on the mixed layer and on mixed layer modeling at annual and seasonal time scales. The fresh water flux across the air-sea interface is the most important factor influencing the salinity of the upper layer of the open ocean. Therefore, fresh water flux should be included in mixed layer models for seasonal and longer time scales, even when temperature appears to be dominant over salinity in the density structure.

To show the effect of salinity for an actual case, the year 1967 at OWS "P" was selected for simulation. To obtain as realistic forcing as possible (when synoptic precipitation observations were unavailable), monthly average precipitation values were obtained from Dorman and Bourke (1979) [Ref. S]. Daily evaporation values were calculated from latent heat fluxes. This calculation showed that evaporation is weakest in the summer, and the highest values were in the fall and winter seasons. Monthly net evaporation exceeds climatological precipitation in May and August only. The calculation of evaporation and precipitation values were only an approximation since no spray effects were considered in the computation. Use of the more realistic estimation of net precipitation over evaporation causes the mixed layer to be 25 meters shallower than the case without fresh water flux, representing a 20% change. Rainfall at OWS "P" is therefore particularly important in keeping the mixed layer relatively shallow during the late fall and winter. The results were comparable to the hypothetical forcing of a constant P-E of 0.5 m year. The addition of salinity forcing also changed the predicted mixed layer temperature, even though the surface heat fluxes were unchanged. The biggest temperature difference occurs in the summer. The difference is especially pronounced after early April through the summer, after which it decreases until the end of the year. Mixed layer salinity shows a -0.28 ppm change over the whole year showing that a small long-term advective source of salinity is needed for a climatological balance to be maintained.

In a similar manner, time series of the differences of salinity, temperature and MLD between the cases with and without precipitation and evaporation were calculated. Calculation of the differences in MLD, temperature and salinity relative to the annual simulation with no surface salinity flux revealed two dominant time scales, the diurnal cycle and the seasonal cycle. The seasonal cycle was considered more important in this study. The seasonal trend is very similar to the hypothetical case with a constant value of precipitation-evaporation of 0.5 m year.

63

Although the salinity change is small, approximately 0.1 ppm, there is a large effect on the MLD, showing a difference of 25 meters at the end of the year. The temperature is a half degree warmer than for the case without rainfall. The small trend in salinity needs to be balanced by horizontal advection and or vertical diffusion in the model. This trend was subtracted from the computed values of surface salinity in order to compare the predicted annual salinity cycle with climatology. Although horizontal advection and diffusion are neglected and precipitation is only approximated, the results are consistent with expected statistical variations. The phase of salinity climatology with the predicted salinity is particularly consistent. The best actual agreement is between January and July. After this the model over-predicts the rise in salinity.

Future work is recommended, in this study especially including more realistic values of precipitation and evaporation. This may be possible by taking into consideration the amount of cloud cover and also the wind stress in order to derive an effective parameterization for synoptic-scale precipitation. Horizontal advection and vertical diffusion should also be included in future modeling to get a more realistic approximation to the interplay between mixed layer and large-scale circulation dynamics at Ocean Weather Station P".

LIST OF REFERENCES

1. Garwood, Roland, 1977. *An Oceanic Mixed Layer Model Capable of Simulating Cyclic States.* J. Phys. Oceanogr., 7,455 - 468.

2. Kraus, E. B. and J. S. Turner, 1967. *A one-dimensional model of the seasonal thermocline. II. The general theory and its consequences.* Tellus., 19, 98-106.

3. Denman, K. L., 1973. *A time-dependent model of the upper ocean.* J. Phys. Oceanogr., 3, 173-184.

4. Denman, K. L., and M. Miyake, 1973. *Upper layer modification at Ocean Station "Papa": Observations and simulation.* J. Phys. Oceanogr., 3, 185-196.

5. Miller, J. R., 1976. *The salinity effect in a mixed layer ocean model.* J. Phys. Oceanogr., 6, 29-35.

6. Paulus Alan Richard, 1978. *Salinity Effects in an Oceanic Mixed-Layer Model.* M.S. Thesis, Naval Postgraduate School, Monterey, Ca. 77 pp.

7. Robinson K. Margaret, 1976. *Atlas of north Pacific Ocean monthly mean temperatures and mean salinities of the surface layer.* Naval Oceanographic Office Reference Publication 2.

8. Dorman, C. E., and R. H. Bourke, 1979. *Precipitation over the Pacific Ocean, 30°S to 60°N.* Mon. Wea. Rev., 107, 896 - 910.

9. Dodimed A.J., Favorite F., Hirano T., 1962. *Review of Oceanography of the Subarctic Pacific Region.* October 1, 1962. 105 pp.

10. Tabata Susumu, 1961. *Temporal changes of salinity, temperature and dissolved oxygen content of the water at Station "P" in the Northeast Pacific Ocean.* J. Fish. Res. Bd. Can., 18 (6), 1073-124.

11. Tabata Susumu, 1965. *Variability of oceanographic conditions at Ocean Station "P" in the northeast Pacific Ocean.* J. Fish. Res. Bd. Can., III: series IV: June 1965, 367-418.

12. Meteorological Branch, 1961. *Monthly and 10-year means of meteorological parameters at Ocean Station "P"--Jan. 1951-Dec. 1960 inclusive.* (Climatology Division, Department of Transport of Canada; unpublished).

13. Tully, J. P., and Allen J. Dodimead, 1957. *Canadian oceanographic research in the Northeast Pacific Ocean.* MS Rept., Fish. Res. Bd. Canada Pacific Oceanographic Group, 11 pp., 18 fig. (Unpubl.)

14. Dodimead, A. J., 1958. *Report on oceanographic investigations in the northeast Pacific Ocean during August 1956, February 1957, and August 1957.* Fish. Res. Bd. Canada MS Rept. Series (Oceanogr. and Limnol.) No. 20, 14 pp., 35 fig.

INITIAL DISTRIBUTION LIST

		No. Copies
1.	Defense Technical Information Center Cameron Station Alexandria, VA 22304-6145	2
2.	Library, Code 0142 Naval Postgraduate School Monterey, CA 93943-5002	2
3.	Professor E. B. Thornton, Chairman Department of Oceanography Naval Postgraduate School Monterey, CA 93943	1
4.	Professor R. W. Garwood, Code 68Gd Department of Oceanography Naval Postgraduate School Monterey, CA 93943	5
5.	Professor R. L. Haney, Code 63Hy Department of Meteorology Naval Postgraduate School Monterey, CA 93943	1
6.	Professor P. Gallacher, Code 68Ga Department of Oceanography Naval Postgraduate School Monterey, CA 93943	1
7.	Professor R.H. Bourke, Code 68Bf Department of Oceanography Naval Postgraduate School Monterey, CA 93943	1
8.	Direccion General de Estudios Primera Zona Naval Guayaquil Ecuador	1
9.	Instituto Oceanografico de la Armada Base Naval Sur P. O. Box 5940 Guayaquil Ecuador	1
10.	Escuela Politecnica del Litoral Guayaquil Ecuador via:	1

Instituto Oceanografico de la Armada
Base Naval Sur
P. O. Box 5940
Guayaquil Ecuador
1

11. Instituto Nacional de Pesca
Letamendi 102 y la Ria
P.O. Box 5918
Guayaquil Ecuador
1

12. Universidad Estatal de Guayaquil Biblioteca
P.O. Box 471
Guayaquil Ecuador
1

13. Universidad Laica de Guayaquil
Guayaquil Ecuador
via:
Instituto Oceanografico de la Armada
Base Naval Sur
P. O. Box 5940
Guayaquil Ecuador
1

1

14. Universidad Catolica de Guayaquil
Guayaquil Ecuador
via:
Instituto Oceanografico de la Armada
Base Naval Sur
P. O. Box 5940
Guayaquil Ecuador
1

1

15. Instituto Geografico Militar
Quito Ecuador
via:
Instituto Oceanografico de la Armada
Base Naval Sur
P. O. Box 5940
Guayaquil Ecuador
1

1

16. Fuerza Aerea Ecuatoriana
Departamento de Meteorologia
Ministerio de Defensa Nacional
Quito Ecuador
1

17. Autoridad Portuaria de Guayaquil
Guayaquil Ecuador.
via:
Instituto Oceanografico de la Armada
Base Naval Sur
P. O. Box 5940
Guayaquil Ecuador
1

1

18. Doctor Manuel Cruz P.   1
    Universidad Estatal de Guayaquil
    P.O. Box 471
    Guayaquil Ecuador

19. Jane Kogelshatz.   1
    Duke Marine Lab
    Beaufort, NC 28516

20. Rich Schramm.   1
    College of Oceanography
    Oregon State University
    Corvallis, OR 97331

21. LT J.G. Galo Garzon   2
    Instituto Oceanografico de la Armada
    Base Naval Sur
    P. O. Box 5940
    Guayaquil Ecuador

22. Dr. Donald Hansen   1
    Ocean. and Met. Lab. NOOA
    4301 Rickenbacker Causeway
    Miami, FL 33149

END

10-87

DTIC